ESRF NEWSLETTER

JULY 1997 EUROPEAN SYNCHROTRON RADIATION FACILITY N° 29

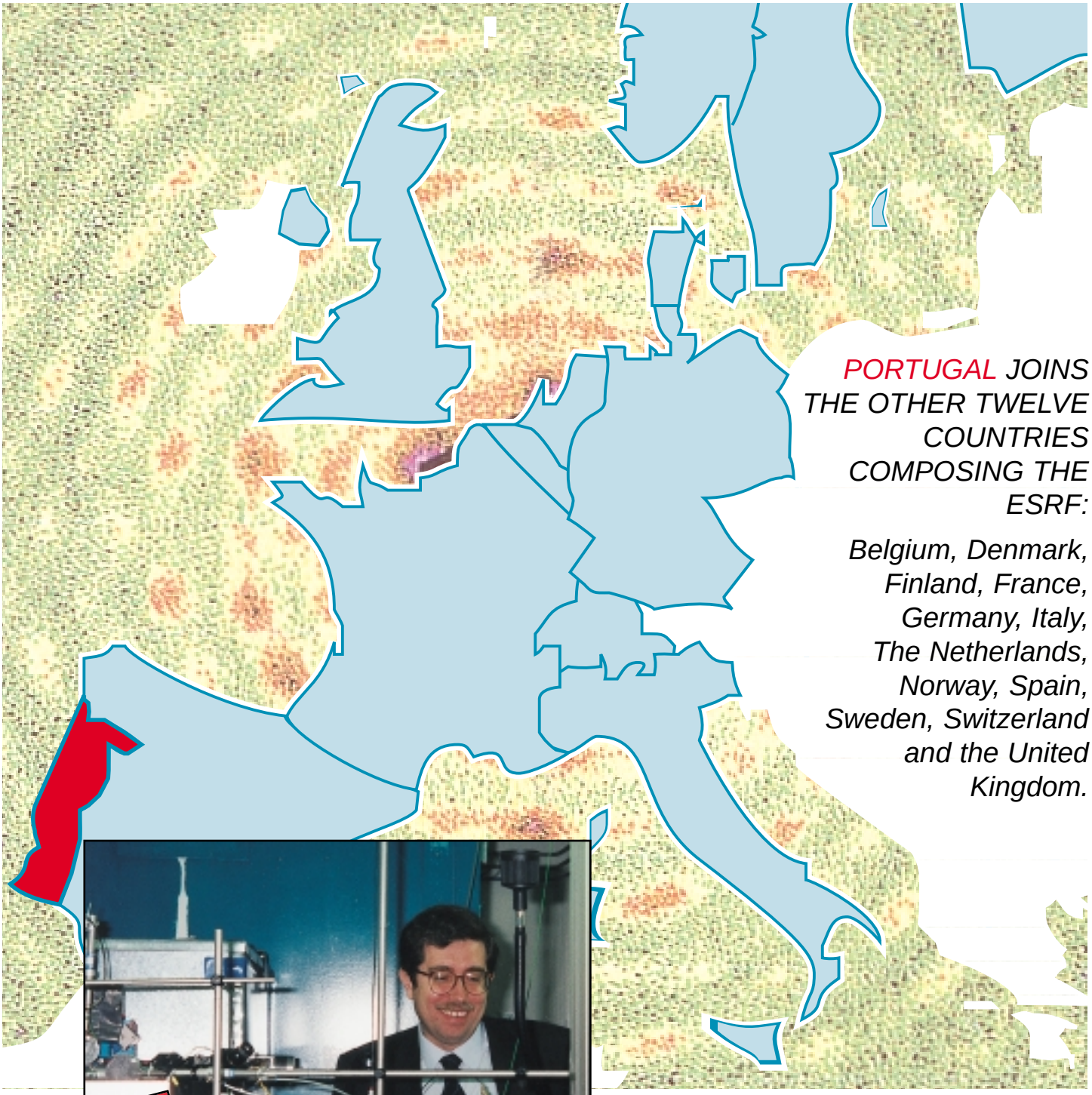

PORTUGAL JOINS THE OTHER TWELVE COUNTRIES COMPOSING THE ESRF:

Belgium, Denmark, Finland, France, Germany, Italy, The Netherlands, Norway, Spain, Sweden, Switzerland and the United Kingdom.

J.M. GAGO, the Portuguese Minister for Science and Technology, visited the ESRF on 16 May 1997.

ISSN 1011-9310

CONTENTS

Photography by:
C. Argoud.

ABOUT THE NEWSLETTER...

The ESRF Newsletter is published three times per year and is distributed free of charge to 7000 laboratories and scientists throughout the world.
If you wish to receive it regularly, please fill out the form below. You will also then receive the ESRF Highlights free of charge each year in the autumn.
The Newsletter, as well as the Highlights and the Annual Report, can be found on the Web at http://www.esrf.fr.

Name: .....

Company name: .....

Address: .....

PO box: .....

Country: .....

Please send to:
ESRF • Information Office
BP 220 • F-38043 Grenoble Cedex 9 • FRANCE
Fax: +33 76 88 24 18

The Newsletter is published by the ESRF.
Editor: D. Cornuéjols
BP 220, F-38043 Grenoble cedex 9 (France)
e-mail: information@esrf.fr
Tel (33) 4 76 88 20 25

Dépôt légal : 3ème trimestre 1997. Printed in France by Repro-Express. Layout by Pixel Project.

PORTUGAL JOINS THE ESRF

The government of Portugal has expressed its interest in joining the ESRF as a Scientific Associate with a view to move to full membership once the involvement of the Portuguese scientific community in the ESRF has increased appropriately.
The ESRF Council has agreed that an arrangement on the long-term use of synchrotron radiation is made between the ESRF and the government of Portugal and has authorised the Director General to enter into detailed negotiations on this item with the aim of admitting Portugal as a Scientific Associate with effect from 1 January 1998.

The ESRF Statutes stipulate that each Member to the ESRF shall hold at least 4% of the shares. This has led some of the Contracting Parties to form consortia such as Benesync (Belgium, The Netherlands) or Nordsync (Denmark, Finland, Norway, Sweden). However, the ESRF Convention also provides for another option of access suited for countries with relatively small scientific communities, namely "arrangements for long-term use of synchrotron radiation". At the end of 1996, the ESRF Council formalised this option by establishing a model arrangement with so-called Scientific Associates. Portugal is the first of several interested countries to make use of this access possibility.

In preparing for this associateship, a delegation of eighteen Portuguese scientists visited the ESRF on 5 April 1997, followed by the visit of Professor J.M. Gago, the Portuguese Minister for Science and Technology, on 16 May 1997.

Although the Portuguese government would have preferred full Membership in its own right, a share of 4% was not realistic given the present size of the Portuguese scientific community. Therefore, the status of Scientific Associate was chosen as a first step towards joining the ESRF. Meanwhile, the ESRF Council will start to discuss the question as to whether a reduction of the threshold for Membership to below 4% should be considered in the long term, e.g. after the end of the construction period (1988-1998).

In order that the community of users in Portugal can take full advantage of the ESRF it is planned that the ESRF and the Portuguese community set up a joint scientific committee. Its role would be to give advice to the Portuguese authorities on the development of research in Portugal related to the ESRF and on the allocation of national research funds in the areas where synchrotron radiation is an important research tool.

Pr. J.M. Gago, Portuguese Minister for Science and Technology, in discussion with Pr. Petroff, ESRF Director General.

26TH COUNCIL MEETING

The 26th meeting of the ESRF Council was held in Grenoble on 10 and 11 June 1997. This time, the most eagerly awaited decision came under «Personnel matters»: the Council decided to offer Y. Petroff an extension of his appointment as **Director General** by three years, i.e. up to 31 December 2000.

The Council's approval of an arrangement with **Portugal** to become Scientific Associate as from 1 January 1998, is commented above.

The Council approved the establishment of a **Spanish Collaborating Research Group beamline** at the ESRF, thus bringing the number of CRG beamlines to nine (with altogether 13 independent run stations).

The **financial planning** presented by Management which, for the coming years, provides for an increase of Members' contributions in line with the assumed inflation index (i.e. implying constant purchasing power) was only taken note of. The Council asked Management to prepare an alternative proposal to the 1998 budget, providing for 390 million French francs of new Members' contributions (= same amount as 1997).

The Council (re-)appointed **Chairmen (and Vice-Chairmen)** of the

- Audit Committee / Administrative and Finance Committee: J.F. Conscience, (U.M. Grassano),
- Purchasing Committee: G. Luijckx, (S. Romo),
- Science Advisory Committee: R. Fourme, (M. Fuess),
- and, with effect from 1 January 1998, of the Council: G. von Klitzing, (P. Zinsli).

34TH MEETING OF THE SCIENCE ADVISORY COMMITTEE

On 15 and 16 May 1997, the Science Advisory Committee (SAC) met for the first time in its new composition (cf. ESRF Newsletter N° 27, p. 3).

As has now become regular practice, on the first half-day of their meeting the members of the SAC heard a series of presentations from ESRF staff and CRG members on recent scientific results and technical achievements (e.g. on the availability of high-energy photos up to 1 MeV, microdiffraction, X-ray optics and the solution of protein structures by using the MAD technique).

During the meeting proper, the SAC
• discussed Management's report and, in this context, was impressed by the continuous development of undulators and the prospects of the last one of the 30 ESRF beamlines (inelastic scattering) whose construction will begin mid-1997;
• recalled the SAC's recommendation for a beamline 31 for low-energy applications, which is currently suspended due to budget and manpower constraints;
• appreciated the activity of the ESRF Users' Organisation, which was well presented by its present chairwoman, Sakura Pascarelli, as being very positive and allowing a smooth and efficient operation of the ESRF;
• studied the proposal for a Spanish multi-purpose CRG beamline and recommended the Council to approve this project while at the same time recommending more coordination between the then 10 materials science-oriented CRGs;
• discussed reports from the Review Committees on the last round of beam time applications and recommended rules for the management of long-term applications for beam time which must be well justified by their nature and quality and,
• in the framework of the review of beamlines, noted the actions resulting from previous reports, discussed three new reports from beamline Review Committees and established a plan for further reviews. The recommendations of these review panels will form the basis for refurbishment and improvement of beamlines.

Finally, the SAC nominated a Chairman (R. Fourme) and a Vice-Chairman (H. Fuess) (subsequently appointed by the Council) and recommended the Council to involve the SAC in the selection procedure of the Director General and the Research Directors.

THE DIRECTOR GENERAL OF THE ESRF IS ASSISTED BY FOUR DIRECTORS:
THE MACHINE DIRECTOR, TWO RESEARCH DIRECTORS AND THE DIRECTOR OF ADMINISTRATION.
FOR THE PERIOD FROM 1 OCTOBER 1998 ONWARDS, THE ESRF IS SEEKING TO RECRUIT ITS

DIRECTOR OF ADMINISTRATION

The function

The Director of Administration is charged with the organisation of the administrative work related to the operation of the company. This includes all administrative and legal connections with outside companies, institutes and corporate members of the ESRF. He/she advises the Director General, the other Directors and the Heads of the Technical Services and Computing Services Divisions on administrative, procedural and legal matters.

The Director of Administration leads the Administration Division (36 posts) and is responsible for the establishment and operation of its budget, and for the recruitment and supervision of its staff.

In relation to the operation of the company, he/she is responsible for:
• advising the Director General on and co-ordinating proposals for the company's annual budget and staffing plan,
• advising the Director General on the formulation of medium-term financial and staffing estimates,
• supporting the Council, its Administrative Committees and any sub-committees and working groups concerned with administrative matters that are set up by the Council,
• development of administrative systems,
• liaison with the Unions and the elected representatives of the staff,
• any other tasks or responsibilities which may be assigned by the Director General.

Qualifications and experience

The successful candidate should have:
• professional qualification in economics, law or science,
• well-developed conceptual and organisational skills,
• experience in a similar post,
• working knowledge of English and some French (any other European language would be an asset).

The successful candidate will have the full support and assistance of the Directorate as well as substantial independence in the fulfilment of his/her tasks.

The contract is to begin on 1 October 1998 and will be for a period of up to five years.

Individuals wishing to apply their conceptual skills, knowledge and experience in the operation of the ESRF should send their written applications by 1 October 1997 to the:

Chairman of the ESRF Council
BP 220
F-38043 Grenoble Cedex 9
France

Recent Proposal Reviews: Results

Scientists interested in carrying out experiments on ESRF beamlines submitted a total of 678 applications for beam time for the recent 1 March deadline. They were applying for beam time on the 27 ESRF and 5 CRG beamlines which will be scheduling user experiments between July and December 1997. Following the meetings of the Review Committees at the ESRF late in April, 294 proposals were selected and allocated a total of 3759 shifts of beam time. The distribution of proposals submitted and allocated, by scientific area, is as **Table 1**:

Slightly more than 43% of the applications were successful this round when averaged across the different scientific areas; this compares with a mean success rate of 45% over previous rounds.

The number of shifts requested and allocated, per Review Committee, are shown for the current proposal round in **Figure 1**. **Figure 2** shows the number of shifts allocated compared with shifts requested, per scheduling period, since the beginning of operation with users in September 1994. It should be noted that the second scheduling period during each year is slightly shorter than the first, so that there are proportionately fewer shifts allocated and scheduled for user experiments during the second half of each year.

The beamlines most heavily in demand this round were ID16, for X-ray inelastic scattering, ID12B, the Dragon with polarisation selectivity, ID10, the Troika beamline, and ID2, which combines SAXS and biocrystallography applications.

Prospective users are advised that the next deadline for proposals, for beam time between January and June 1998, is

1 September 1997

Further details, including beamlines open for experiments and applications for long term projects for the next scheduling period, will be available from July on the World Wide Web at the ESRF address: http://www.esrf.fr.

R. Mason

Review Committees	*Proposals submitted*	*Proposals accepted*
Chemistry	*102*	*41*
Hard Condensed Matter: Elect. & Magn. Properties	*104*	*55*
Hard Condensed Matter: Structures	*165*	*66*
Life Sciences	*155*	*69*
Methods and Instrumentation	*28*	*17*
Soft Condensed Matter	*68*	*25*
Surfaces and Interfaces	*56*	*21*
Total	*678*	*294*

Table 1

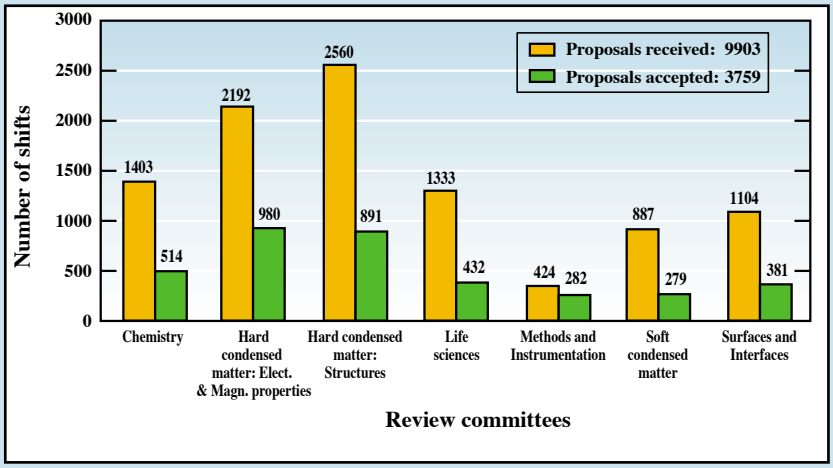

Fig. 1: Number of shifts of beam time requested and allocated, per Review Committee, for the scheduling period July to December 1997.

Fig. 2: Total number of shifts of beam time requested and allocated, per scheduling period, September 1994 to December 1997.

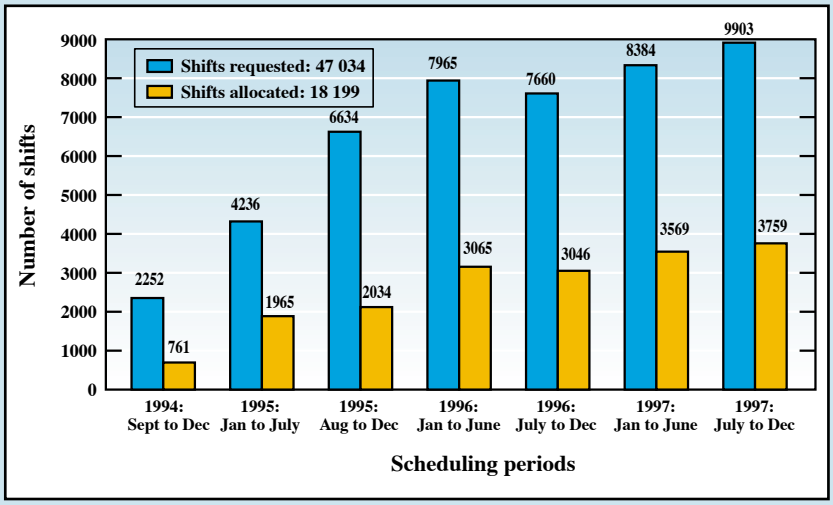

International Conference

Highlights in X-Ray Synchrotron Radiation Research

17 - 20 November 1997

IN CONJONCTION WITH

ESRF Users' Meeting

21 November 1997

ORGANISED BY THE ESRF AT ATRIA WORLD TRADE CENTER, GRENOBLE

List of Invited Speakers at the Main Conference

(as of 20 June 1997)

Some additional speakers may be scheduled for these sessions in the next few months.

D. Andrault (Paris)
J. Baruchel (Grenoble)
B. Batterman (Ithaca)
M. Blume (Brookhaven)
U. Bonse (Dortmund)
E. Burkel (Rostock)
P. Carra (Grenoble)
C-T. Chen (Hsinchu)
M. Cooper (Warwick)
J. Daillant (Saclay)
S. Doniach (Stanford)
S. Ferrer (Grenoble)
J-M. Filhol (Grenoble)
E. Gerdau (Hamburg)
D. Gibbs (Brookhaven)
J. Goedkoop (Grenoble)
J. Gronkowski (Warsaw)
G. Grübel (Grenoble)
W. Hendrickson (New York)
E. Kisker (Düsseldorf)
P. Loubeyre (Paris)
H-K. Mao (Washington)
R. Martin (Urbana)
A. Momose (Saitama)
M. Parrinello (Stuttgart)
A. J. Ryan (Manchester)
G. Sawatzky (Groningen)
J. Schneider (Hamburg)
F. Sette (Grenoble)
S. Sinha (Argonne)
A. Snigirev (Grenoble)
P. Spanne (Grenoble)
M. Stamm (Mainz)
J. Trümper (Garching)
S. W. Wilkins (Melbourne)

List of Invited Speakers at the Structural Biology Symposium on 19 - 20 November

(as of 20 June 1997)

Virus structures
L. Liljas (Uppsala)
M. Rossman (West Lafayette)
D. Stuart (Oxford)

Time-resolved crystallography
J. Hajdu (Uppsala)
K. Moffat (Chicago)
I. Schlichting (Heidelberg)

DNA-replication, transcription, translation and repair
S. Burley (New York)
S. Cusack (Grenoble)
L. Pearl (London)
T. Richmond (Zürich)
T. Steitz (Yale)

Membrane proteins
N. Isaacs (Glasgow)
H. Michel (Frankfurt)
J. Rosenbusch (Basel)
T. Schirmer (Basel)

In this anniversary year, the ESRF is organising an international conference in recognition of the pioneering work performed since the first observation of synchrotron radiation in 1947 and the remarkable results achieved. It will emphasise the new impetus given to this research by the third generation synchrotron radiation sources in the X-ray range, in fields such as magnetism, high pressure, structural biology, imaging and topography, and soft condensed matter.

The scientific programme from Monday 17 - Thursday 20 November is made up of plenary lectures given by invited speakers on the above mentioned topics. These lectures will be followed by poster sessions in the late-afternoon. In parallel, a Structural Biology Symposium will be held on Wednesday 19 - Thursday 20 November and the annual Users' Meeting follows on Friday 21 November.

If you wish to receive the third circular of the Main Conference and Users' Meeting, which includes registration and accommodation forms, and you have not already requested further information, you can still complete the pre-registration form that can be found on the web at **http://www.esrf.fr** or contact the Conference Secretariat.

Deadline for early registration: 15 September 1997

In addition to the Main Conference, satellite meetings are also being organised. Registration for these workshops is done using the SR50 and Users' Meeting registration form. If you have already ticked the relevant boxes on the pre-registration form you will receive information on these workshops automatically.

For specific information concerning the programme of each workshop you should contact:

Magnetism & X-ray Scattering

C. Vettier.
e-mail: SR50@esrf.fr
In e-mail start subject with: MXS

Imaging & High Resolution Diffraction on ID19

J. Baruchel.
e-mail: SR50@esrf.fr
In e-mail start subject with: ID19

Crystallography at High Pressure using S.R.

D. Häusermann.
e-mail: SR50@esrf.fr
In e-mail start subject with: HP

CONTACT:
Conference Secretariat • ESRF • BP220 • F-38043 Grenoble Cedex (France)
Tel: +33 (0)4 76 88 26 80 • Fax: +33 (0)4 76 88 21 60 • E-mail: SR50@esrf.fr • http://www.esrf.fr

VACANCIES AT THE ESRF ON 24 JUNE 1997

	Ref	Subject
SCIENTISTS (5-year contracts)	2203	Troika beamline
	2117	XAFS experiments in the energy dispersive mode
	2167	XAFS experiments on BM29
	2157	Microfocus beamline (ID13)
POST-DOC (2-year contracts)	PDID24	XAFS experiments in the energy dispersive mode
	PDID26	X-ray fluorescence excitation spectroscopy on dilute systems
	PDID10B	Troika II beamline
	PDID9	Time resolved protein crystallography (ID9)
STUDENTS (2-year contract, renewable 1 year)	CFR206	Conditioning of the time structure of synchrotron beams by X-ray optics
	CFR209	X-ray diffraction topography and phase contrast imaging investigations of SOI-structures and SOI-based circuits
	CFR210	Multi-wavelength anomalous dispersion (MAD) methods in macromolecular crystallography
	CFR211	High resolution diffraction studies of powers
ENGINEER	CDD/BPRW	Software engineer
TECHNICIANS	1513	Radiation protection
	6563	Drafstman/woman specialized in buildings
	5505	Software technician
	CDD/GN	Diagnostics technician (m/f) 8 to 9 month-contract
	2540	Beamline technician
ADMINISTRATIVE	2531	Secretary

Experience: Previous postdoctoral experience with synchrotron radiation is essential.

If you are interested, please send us a fax (+33 (0) 4 76 88 24 60) or an e-mail (peritore@esrf.fr) with your address, and we will provide you with an application form. You can also print out an application form on the World Wide Web http://www.esrf.fr

X-Ray Diffraction on Photonic Colloidal Single Crystals

M. Megens[1], C. M. van Kats[1], P. Bösecke[2,3] and W. L. Vos[1]

1 Van der Waals-Zeeman Instituut, Universiteit van Amsterdam (The Netherlands)
2 ESRF, Experiments Division
3 Max Planck Institut, Hamburg (Germany)

We have performed X-ray diffraction on colloidal single crystals with lattice parameters in the order of several hundred nanometers on ID2. These crystals are optical photonic crystals, i.e. crystals that modify the propagation of light and may lead to novel optical phenomena, analogous to semiconductor electronics.

In photonic crystals, the refractive index varies periodically on length scales comparable to optical wavelengths. This has an effect on light similar to the effect that the periodic potential of atomic crystals has on electrons [1,2]. The periodicity causes optical Bragg reflections: directions in the crystal where waves with certain frequencies are reflected. Figure 1 shows a Bragg reflection for green light in a photonic colloidal crystal. If the light is very strongly coupled to the crystal, an optical photonic band gap may occur, i.e. a frequency band in which no light can be transmitted in any direction. This can be interpreted as a Bragg reflection that extends over a full 4π solid angle. Photonic band gaps for light are expected to have unusual properties: spontaneous emission of excited atoms with a resonance in the forbidden frequency band is inhibited, and light can be localised [1]. Thus, with photonic band gap crystals one may achieve control over photons similar to that over electrons in microelectronics [1,2].

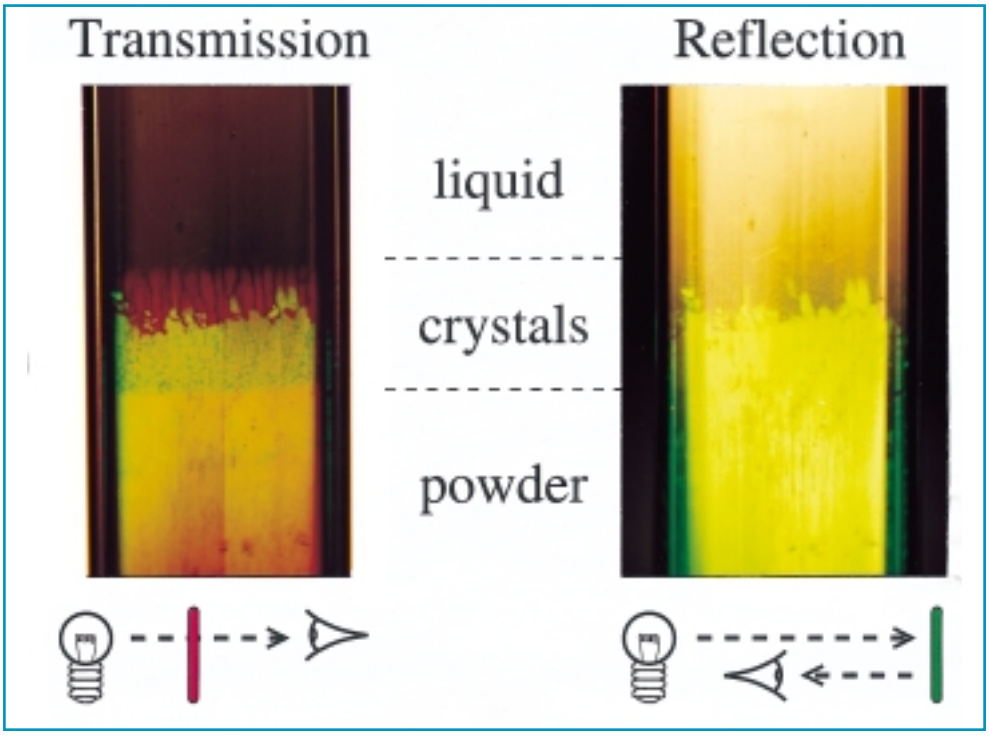

Fig. 1: Photomicrographs of a sample of polystyrene colloids in methanol in a 4 mm wide glass capillary. The pictures were taken with white light, in transmission (left) and reflection (right). The bright green Bragg reflections are caused by the fcc (111) planes oriented parallel to the capillary wall. Red light is still transmitted through the crystals. At the top of the sample, the density of the colloids is lower, hence they form a disordered liquid. This results in random multiple scattering of the light and thus appears dark in transmission and white in reflection.

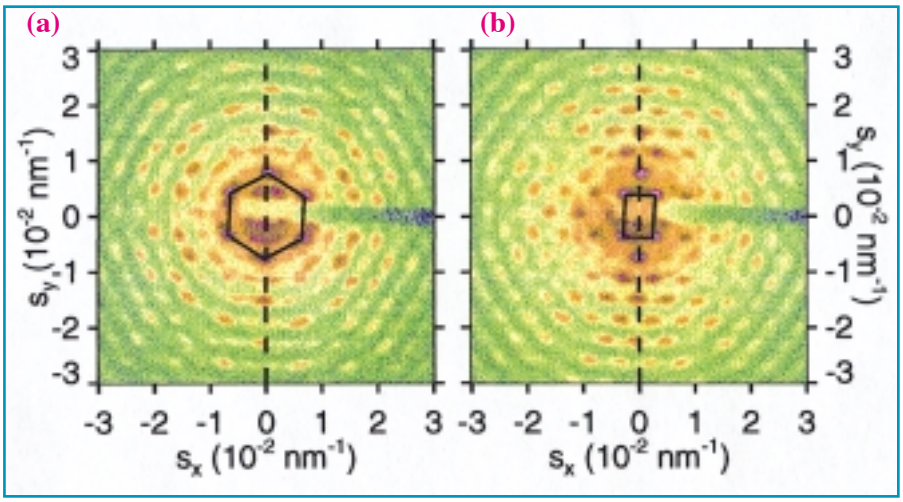

Fig. 2: Small-angle X-ray scattering patterns from a crystal of 242 nm diameter polystyrene colloidal spheres in water. The spheres have formed an fcc crystal with the (111) planes parallel to the wall of the capillary. In (a) the X-ray beam is parallel to a [111] axis. In (b), the X-ray beam is parallel to a [110] axis. The large number of rings further out in the scattering pattern is caused by the form factor of the monodisperse colloidal spheres [3].

The realisation of three-dimensional periodic structures with lattice parameters of the order of optical wavelengths presents a major challenge [2]. We study colloidal suspensions of particles that are so small (10-1000 nm) that they execute Brownian motion. Familiar examples of colloids are fog, milk or paint. It is currently possible to synthesise colloidal spheres with a very small variation in size [3]. Such colloids can self-organise into bulk three-dimensional crystals, that are a natural realisation of photonic crystals for light. Thus, colloidal crystals are promising building blocks for crystals with optical photonic band gaps.

Because the optical properties of photonic crystals are intimately related to the crystal structure, it is crucial to know their structure [4]. Usual optical techniques such as light scattering and microscopy are not suited for photonic crystals however, for several reasons. First, a strong interaction between the light and the crystals results in multiple scattering. We have observed that the Bragg spacings then strongly deviate from the real lattice spacings [5]. Second, the required lattice spacings allow only a few Bragg reflections to be observed in the available optical spectrum. These points are remedied by small-angle X-ray scattering. Beamline ID2 has several key features for X-ray diffraction experiments on photonic colloidal crystals: the narrow focus allows a single crystal to be isolated for study, and the high brilliance allows experiments in reasonably time scales.

Figure 2 presents X-ray diffraction patterns from a colloidal single crystal [6]. The diffraction patterns show symmetric patterns of Bragg peaks, thus the spheres are ordered in a crystalline array. If we translate the sample relative to the X-ray beam, we observe doubling or tripling of each peak or even powder rings, which means that the beam then irradiates two, three, or many crystallites respectively. This confirms that the diffraction patterns in Figure 2 indeed result from a large single crystal, with a size larger than the beam diameter (0.2 x 0.5 mm). The diffraction peaks are well explained with an fcc structure with a lattice parameter of 370 nm, a remarkable value for an X-ray diffraction study.

We see many Bragg spots simultaneously in Figure 2, in contrast to usual single crystal X-ray studies on atomic crystals. The reason is that the X-ray wavelength is much smaller than the lattice spacing, hence the Ewald sphere is almost a plane. This Ewald "plane" simultaneously intersects many reciprocal lattice vectors. By rotating the sample, we sweep the Ewald "plane" through reciprocal space (cf. Figure 2). For Figure 2a, the X-ray beam was perpendicular to the window of the sample, while for Figure 2b, the sample was rotated 34° around the long axis of the capillary (vertical), which results in a very different diffraction pattern. The pattern in Figure 2a has approximately a six fold symmetry, which is expected because dense colloids often arrange in hexagonal planes (fcc 111) parallel to a window. The pattern in Figure 2b is characteristic of an fcc crystal aligned with the 110 planes perpendicular to the beam. Such a pattern has not been observed before [6].

In previous experiments on dense charge stabilised colloids, random stacks of hexagonal planes or glass formation have been observed. The present observation of fcc agrees with *a priori* statistical physical predictions. The observation of the fcc structure is exciting for photonics, because theoretical calculations show that photonic band gaps can be made with this structure. To achieve photonic band gaps, crystals must be made of materials with high refractive indices, which we are currently pursuing.

The present experiments demonstrate that X-ray diffraction is a powerful tool to investigate systems with length scales comparable with optical wavelengths. In particular the two-dimensional detection is an attractive feature as shown in Figure 2. The large number of diffraction peaks in Figure 2 suggest that the Debye-Waller factors of the crystals are small and that the particles never wander far from their lattice positions. It is expected that a detailed study of the Debye-Waller factors will provide information about the mesoscopic interparticle forces, which are currently a subject of debate. ■

References

[1] C.M. Soukoulis (ed.) Photonic Band Gap Materials (Kluwer, Dordrecht, 1996).

[2] J.D. Joannopoulos, P.R. Villeneuve and S. Fan, Nature 386, 143 (1997).

[3] M. Megens, C.M. van Kats, P. Bösecke and W.L. Vos, J. Appl. Cryst (1997, at press); Langmuir (submitted).

[4] W.L. Vos, M. Megens, C.M. van Kats and P. Bösecke, J.Phys. Cond. Matter 8, 9503 (1996).

[5] W.L. Vos, R. Sprik, A. van Blaaderen, A. Imhof, A. Lagendijk and G.H. Wegdam, Phys. Rev. B 53, 16231 (1996); In Ref. [1], p. 107.

[6] W.L. Vos, M. Megens, C.M. van Kats and P. Bösecke, Langmuir (accepted).

FLUCTUATIONS OF FREELY-SUSPENDED SMECTIC FILMS AS OBSERVED BY DIFFUSE X-RAY REFLECTIVITY

W.H. DE JEU[1], E.A.L. MOL[1], G.C.L. WONG[1], J.-M. PETIT[2] AND F. RIEUTORD[2]

1 FOM-INSTITUTE FOR ATOMIC AND MOLECULAR PHYSICS, AMSTERDAM (THE NETHERLANDS)
2 BM32 CRG (IF) AT THE ESRF

The possibilities to measure the diffuse X-ray reflectivity of interfaces and thin films are only being fully developed thanks to synchrotron sources. At BM32 during the experiment, we could determine the spectral dependence of the thermal fluctuations in freely-suspended smectic liquid crystalline films down to molecular dimensions. While at long wavelengths the top and bottom of such a film fluctuate in unison, at shorter wavelengths a cross-over to independent fluctuations could be observed.

FLUCTUATIONS IN LESS THAN 3-D

Long-range translational order is a defining quality of 3-D crystals; it leads to the existence of Bragg reflections. It is well known that such a translational periodicity is destroyed by thermal fluctuations in 2-D and 1-D systems. However, we do not need a low-dimensional world to observe such effects; similar arguments apply in 3-D to smectic liquid crystals. These consist of stacks of fluid monolayers, where rod-like molecules order into a density wave along one direction, but remain fluid in the other two (Figure 1). In such a system the '1-D' translational order of the fluid layers is not truly long-range but decays algebraically with relative position as $\mathbf{r}^{-\eta}$. This is due to the fluctuations of the smectic layers: if $u(\mathbf{r})$ is the layer displacement from its equilibrium position, $\langle u^2(\mathbf{r})\rangle$ diverges logarithmically with the sample size [1] (see intermezzo).

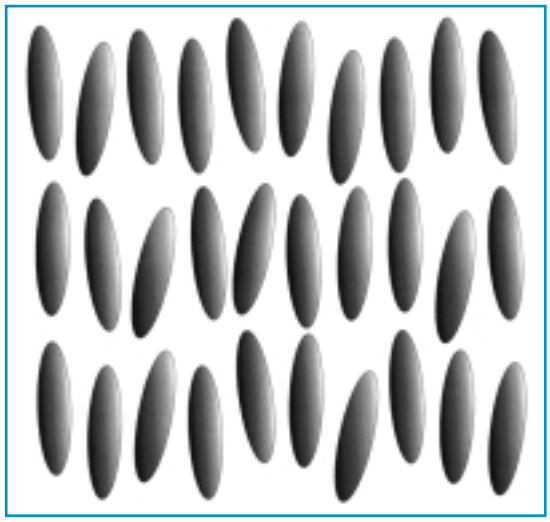

Fig. 1: Stacks of fluid layers forming a smectic phase.

FREELY-SUSPENDED SMECTIC FILMS

A unique property of smectic liquid crystals is their ability to form films that are freely suspended over an aperture in a frame. In such a film the smectic layers align with a high degree of uniformity parallel to the two flat air-film interfaces. To accomplish X-ray reflectivity measurements – which give a large footprint at small incident angles – we succeeded in making films as large as 1 x 3 cm^2 [2]. Even for such areas, the film thickness L can be easily varied from several hundreds of molecular layers (some μm and thus essentially bulk systems) down to two layers (typically 5-6 nm). Because of these properties, freely-suspended smectic films constitute ideal model systems.

CONFORMAL AND INDEPENDENT FLUCTUATIONS

Similarly to rough surfaces [3], the thermal fluctuations of the smectic layers in a film give rise to diffuse scattering off the specular ridge. The

spectral dependence of the intensity is determined by the layer displacement function $\langle u^2(0,z)\rangle$ and the interlayer displacement-displacement correlation function $C(\mathbf{R},z,z') = \langle u^2(\mathbf{R},z)u^2(0,z')\rangle$, where **R** is in the plane of the film and z along the normal [4], via the surface tension γ and the elastic constants B and K (see intermezzo). At long in-plane length scales $R > R_c$ all the layers are found to fluctuate conformally, i.e. they move in unison [2]. For $R < R_c$ such a conformality is expected to vanish (see bottom of Figure 2), starting between top and bottom of the film [4]. In general, $R_c \approx \sqrt{L/B}$, hence loss of conformality can be expected at large in-plane wave vectors (small R) for thick films and/or systems with a small value of B.

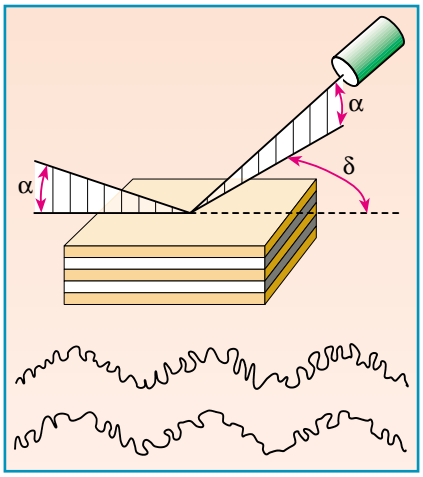

Fig. 2: Top: freely-suspended smectic film and X-ray scattering configuration. Bottom: conformal and independent fluctuations of top and bottom at different wavelengths.

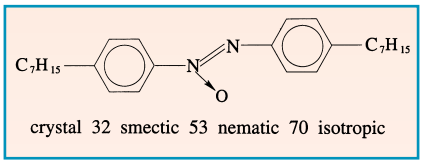

Fig. 3: The compound 7AB and its phase transitions (°C).

EXPERIMENTAL

Using a (2 + 2) surface scattering configuration, the diffuse reflectivity has been probed along q_y, normal to the (q_z, q_x) scattering plane (see Figure 2). Hence the detector was moved out of this plane, keeping the incoming and outgoing angle in the plane constant. The liquid crystalline compound used was *p,p'*-diheptylazoxybenzene (7AB) (see Figure 3). We worked about 0.5 °C below the second-order smectic-nematic phase transition where B can be expected to become small, and with two film thicknesses (24 and 100 layers). The observed intensity is essentially the Fourier transform of $C(\mathbf{R},z,z')$ [2, 3].

RESULTS OF THE SPECULAR AND DIFFUSE REFLECTIVITY

Specular (along q_z at $q_y = 0$) and diffuse longitudinal scans (along q_z at constant q_y) for a 24-layer film are presented in Figure 4a. At small q_y the film is conformal and the diffuse scattering is the coherent superposition of scattering from each layer, showing maxima and minima at the same positions as the specular reflectivity [5]. The disappearance of the interference fringes at large q_y indicates that the top and bottom of the film no longer fluctuate in unison. At the same point the broadening and weakening of the Bragg peak reveals that less than the total number of layers contributes coherently to the diffuse signal. The similar slopes of the transverse diffuse scans at the Bragg peak and its subharmonic (Figure 4b) indicate that lateral correlations between adjacent and next nearest layers persist down to molecular length scales. At the same time the very different slope of the scan at $q_z = 0.7q_o$ confirms the absence of conformality between the top and bottom of the film. A more quantitative description is given elsewhere [6].

INTERMEZZO: SMECTIC LAYER FLUCTUATIONS

In smectic liquid crystals two types of layer deformation play a role.

- Bending of the liquid layers (stiffness constant K), during which the layer spacing is maintained (**Figure A**).
- Compression and dilatation of the layers (constant B, **Figure B**).

The energetics of these two effects can be expressed in the Landau-De Gennes free-energy density:

$$f = \tfrac{1}{2}B\left(\frac{\partial u}{\partial z}\right)^2 + \tfrac{1}{2}K\left(\frac{\partial^2 u}{\partial x^2} + \frac{\partial^2 u}{\partial y^2}\right)^2$$

Expanding u(r) in a Fourier series leads to an expression for the free energy density in terms of the modes of the wave vector q. Next the equipartition theorem can be used to assign an energy 1/2 kBT to each mode. Integrating over all modes leads to the expression for the mean-squared layer fluctuations:

$$\langle u^2(r)\rangle = \frac{k_B T}{8\pi\sqrt{BK}}\ln\left(\frac{L}{d}\right)$$

Here L is the sample size and d the smectic layer spacing. Hence introducing the number of layers N=L/d, the divergence takes the form ln(N).

Fig. A

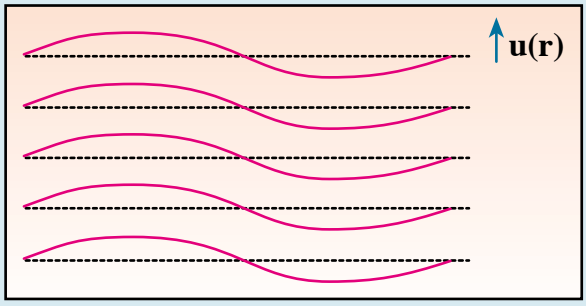

Fig. B

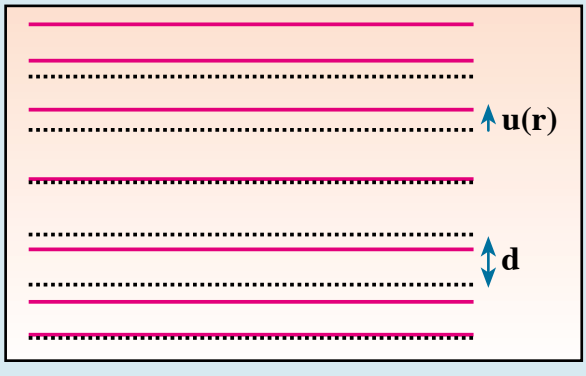

CONCLUSIONS

A cross-over from conformal to independent fluctuations has been observed in freely-suspended smectic films. The (2 + 2) scattering geometry to measure the diffuse scattering in combination with the large dynamic range (> 2 x 10^{10}) at BM32 allowed us to probe wave vectors down to inverse lateral distances between molecules. ■

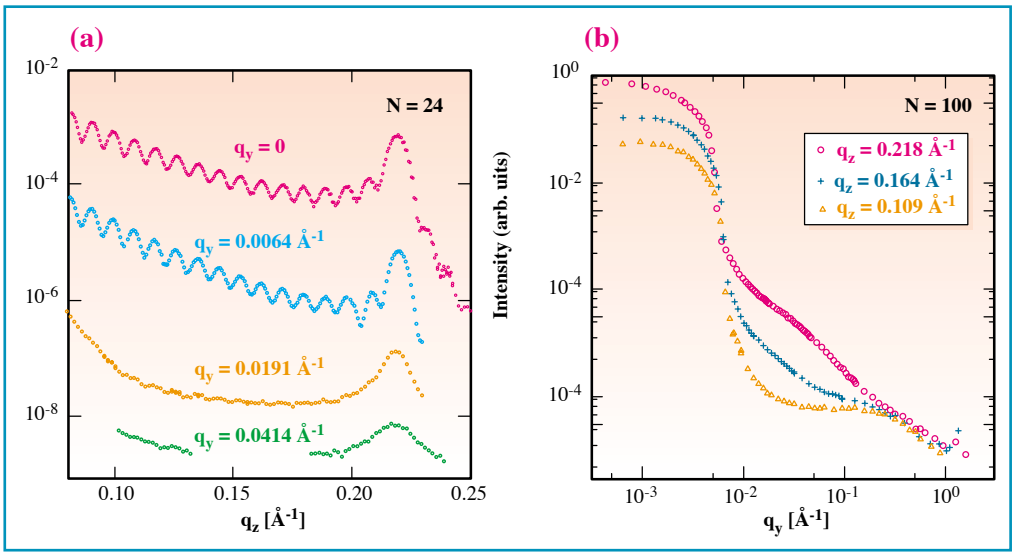

Fig. 4: (a) Longitudinal diffuse scans of a 24 layer film. (b) Transverse diffuse scans (100 layer film) at the Bragg peak ($q_z = q_o$) (red curve), at a subharmonic ($q_z = 0.5q_o$) (blue curve), and at an intermediate position $q_z = (0.7q_o)$ (orange curve).

References

[1] For a recent overview see P.M. Chaikin and T.C. Lubensky, Principles of Condensed Matter Physics (Cambridge University Press, New York, 1995).

[2] E.A.L. Mol, J.D. Shindler, A.N. Shalaginov, and W.H. de Jeu, Phys. Rev. E **54**, 536 (1996).

[3] S.K. Sinha, E.B. Sirota, S Garoff, and H.B. Stanley, Phys. Rev. B **38**, 2297 (1988).

[4] R. Holyst, Phys. Rev. A **44**, 3692 (1991); A.N. Shalaginov and V P. Romanov, Phys. Rev. E **48**, 1073 (1993).

[5] S.K. Sinha, Physica B **173**, 25 (1991).

[6] E.A.L. Mol, G.C.L. Wong, J.-M. Petit, F. Rieutord and W.H. de Jeu, Phys. Rev. Lett. (submitted).

Structure Determination of an Organic Superconductor by High-Resolution Powder Diffraction

From left to right: A.N. Fitch, S.O. Svensson, M. lorenzen, H. Müller.

A.N. Fitch, S.O. Svensson, H. Müller, M. Lorenzen and D.G. Xenikos

ESRF, Experiments Division

The high resolution powder diffraction beamline BM16 has been operating for users since May 1996. The beamline is optimised for carrying out powder crystallography - solving and refining of crystal structures from powder specimens - but also has a wide range of materials science applications, such as anomalous scattering studies, measurement of stress and strain (e.g. in alloys used in aerospace), characterisation of microstructure, studies of glasses and amorphous materials, and dynamic in situ measurements of systems undergoing structural evolution with time (e.g. following the structural changes in batteries during the electrochemical charge and discharge cycles).

Structural characterisation from powders is necessary when single crystals of a material are not available, or for carrying out studies under conditions where single crystals fragment, such as after passing through a destructive phase transition. To understand the physical and chemical properties of crystalline solids, knowledge of the crystal structure is indispensable. Many modern materials do not readily form good quality crystals so that the crystal structure may only be determined by powder methods. Furthermore, a single crystal by its very nature may not be truly representative of a bulk specimen, and it is often the powdered form of a material that may be of use and hence of interest, e.g. zeolite catalysts used in the petrochemical industry are always in the form of powders (tonnes of them) and pharmaceutical products frequently come in the form of tablets, which are compressed powders.

Advantages of the BM16 diffractometer include its operating energy range (5 - 40 keV) and its high angular resolution, so that narrow diffraction peaks can be measured using short-wavelength X-rays. The short wavelengths mean that the sample can be contained in a thin-walled glass capillary without problems of absorption. Spinning the capillary greatly reduces (or eliminates) problems of preferred orientation of needle-like or plate-like crystallites, leading to accurate diffraction intensities. Another advantage is the use of a crystal analyser stage before the detector. Coupled with the high collimation of the incident radiation this leads to the narrow peak widths, but also means that the peak positions are immune to the aberrations present with conventional diffractometers that lead to significant shifts in the measured positions of the diffraction peaks. Hence the positions of the diffraction peaks measured on BM16 are also very accurate. With narrow diffraction peaks whose positions and intensities are accurately known, the diffraction pattern that arises from a complex powder sample can be unravelled to yield an accurate and reliable crystal structure. A recent and interesting example which emphasises some of the features outlined above is the study of the technologically promising, advanced material α_t-$(ET)_2I_3$ [1].

The compound is a superconducting radical cation salt derived from the sulphur heterocycle bis (ethylenedithio) tetrathiafulvalene (BEDT-TTF or ET for short), whose important characteristics are similar to those of commercially used superconducting metal alloys such as NbTi (e.g. superconducting transition temperature T_c, upper critical field Hc2 and critical current density j_c).

The organic superconductor α_t-$(ET)_2I_3$ ($T_c \approx 8$ K) has been used in the manufacture of prototypic devices, such as superconducting films [5-7].

Recent attempts to employ the compound for the fabrication of superconducting composites are undoubtedly a field of enormous commercial potential, since they could make available polymers which retain their specific material properties, but are electrically conducting at ambient temperature and superconducting at the temperature of liquid helium [8].

A polycrystalline, superconducting product, generally referred to as α_t-$(ET)_2I_3$, [2,3] is obtained by thermal conversion of the organic metal α-$(ET)_2I_3$ [4]. All attempts to determine the structure of α_t-$(ET)_2I_3$ proved futile, a consequence of the poor crystal quality resulting after heat treatment [3,5].

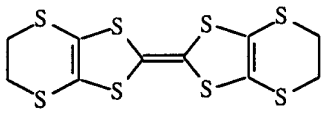

BEDT-TTF OR ET

Recently, we succeeded in performing the first structural characterisation of the superconducting radical cation salt α_t-$(ET)_2I_3$. The compound was synthesised in a phase-pure, microcrystalline form by a newly developed redox process suitable for a large-scale preparation [9]. An SEM-image of the microcrystalline product is displayed in Figure 1.

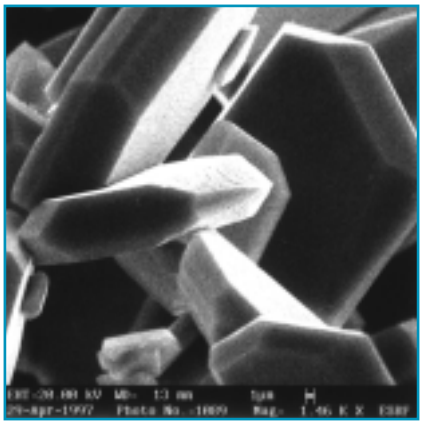

Fig. 1: Microcrystals of α_t-$(ET)_2I_3$.

The powder diffractometer on BM16 (cf. Figure 2) was used to record a high angular resolution X-ray powder diffraction pattern of α_t-$(ET)_2I_3$ at a wavelength of 0.94468(1) Å. The structural model of α_t-$(ET)_2I_3$ was refined with the Rietveld method using the program PC-GSAS [10]. The excellent fit of the peak profiles was obtained using only four peak shape parameters thanks to a special peak shape function [11], although the peaks at low angle are asymmetrical.

Fig. 2: Powder diffractometer on BM16.

A comparison of observed and calculated diffraction patterns is shown in Figure 3. The excellent agreement of observed and calculated profiles clearly demonstrates the presence of a uniform product. Earlier work, based on spectroscopic evidence and Weissenberg photographs, claimed a close structural similarity of α_t-$(ET)_2I_3$ and the related organic superconductors β-$(ET)_2I_3$ (T_c = 1.5 K) [3,5]. The lattice parameters and unit cell volumes of α_t-$(ET)_2I_3$ differ marginally but significantly from those of β-$(ET)_2I_3$ [12,13], which thus could represent a crystallographically distinct phase. The cell volume of fully deuterated α_t-$(ET)_2I_3$ is slightly smaller than that of its protonated counterpart. A reduction of the cell volume as a consequence of hydrogen/deuterium exchange has been observed earlier for ET-based superconductors. [14] It is worth noticing that replacement of hydrogen by deuterium in the ET-molecules enhanced T_c by 0.3 - 0.4 K. The corresponding crystal data are summarised in Table 1.

Table 1: Crystal data (293 K), ESR line widths and transition temperatures T_c of ET phases with the triiodide anion. a Powder diffraction data from this work. The prefix h_8 or d_8 refers to protonated and deuterated ET (donor) molecules, respectively. The figures in parentheses give the standard deviations. b Literature data [11]. c Unoriented powder samples at ambient temperature. d Orientation dependent single crystal data [12].

	α_t-$(h_8$-ET$)_2I_3$[a]	α_t-$(d_8$-ET$)_2I_3$[a]	β-$(ET)_2I_3$[b]
a [Å]	6.6081(2)	6.6093(2)	6.615(1)
b [Å]	9.0878(2)	9.0856(2)	9.100(1)
c [Å]	15.2683(3)	15.2632(3)	15.286(2)
α [°]	94.410(1)	94.452(1)	94.38(1)
β [°]	95.575(1)	95.563(1)	94.41(1)
γ [°]	109.761(1)	109.756(1)	109.78(1)
V [cm³]	852.92(4)	852.55(4)	855.9(2)
Space group	P-1	P-1	P-1
Z	1	1	1
T_c [K]	7.2 - 7.5	7.8 - 7.9	1.4
ΔH_{pp} [G]	23[c]	23[c]	17.6 - 23.35[d]

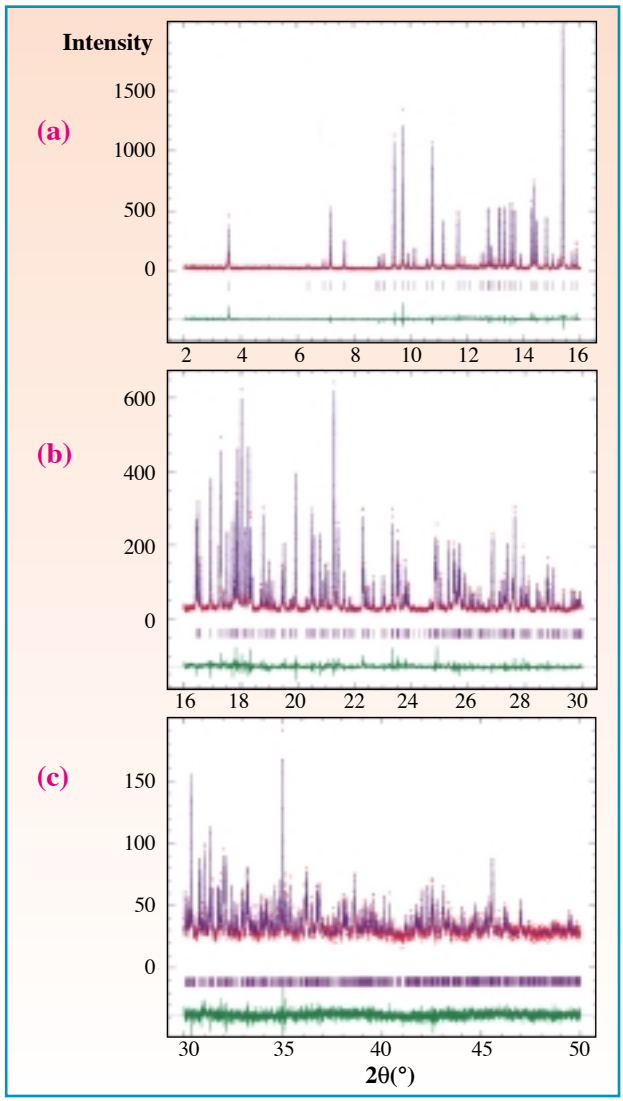

Fig. 3: Diffraction pattern of α_t-$(ET)_2I_3$ ((a) $2 \le 2\,\theta \le 16$ deg; (b) $16 \le 2\,\theta \le 30$ deg; (c) $30 \le 2\,\theta \le 50$ deg) showing the observed (red) and calculated (violet) diffraction patterns, and the differences between them (green). The quality of the fit may be judged by eye to be excellent and yields the Rietveld R-factors $R_p = 0.0813$ and $wR_p = 0.0944$ with a reduced $\chi^2 = 2.4$ for 143 variables. The R-factors give a quantitative indication of the quality of the fit (the lower the R, the better the fit).

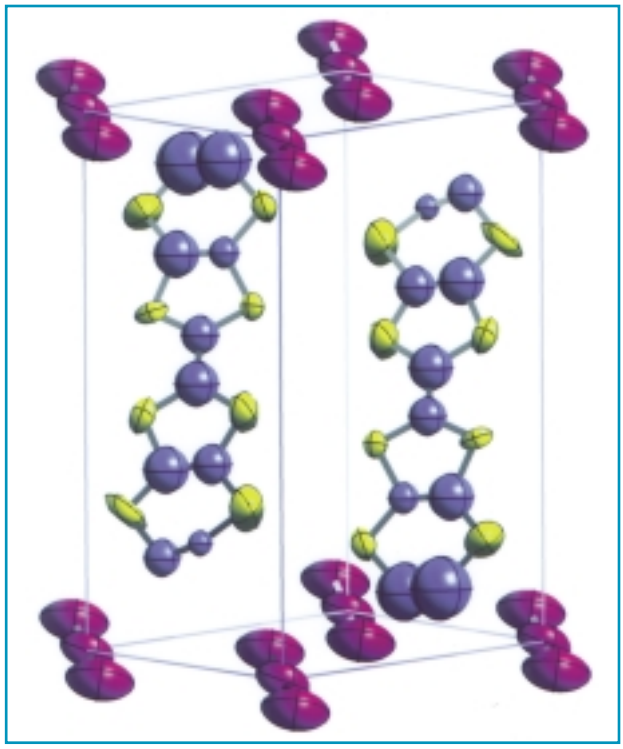

Fig. 4: Crystal structure showing the thermal ellipsoids and unit cell of α_t-$(ET)_2I_3$.

The average crystal structure and unit cell of α_t-$(ET)_2I_3$ are presented in Figure 4. The ET molecules are non-planar and arranged in dimers which form loosely-connected stacks along the crystallographic [110] axis. The carbon atoms at one edge of each ET-molecule show high thermal parameters, indicating disorder of one ethylene group per donor molecule. In view of the structural similarities it is conceivable that the nearly identical cell parameters and packing motifs of the ET-molecules, but strikingly divergent transition temperatures of α_t-$(ET)_2I_3$ (7.1 - 7.9 K) and β-$(ET)_2I_3$ (1.4 K), are linked to small conformational differences. A pressure-induced disorder-order transition of the ethylene groups of β-$(ET)_2I_3$ raises T_c from 1.4 K to 8 K [15]. At present, it is not clear whether the disorder of the end groups in α_t-$(ET)_2I_3$ at ambient temperature is of statistical nature, as in β-$(ET)_2I_3$, [12,13] or rather related to the presence of ordered and disordered domains in the same crystallite. The importance of the end group conformation of the donor molecules and their role on lattice softness, electron phonon coupling and hence the superconducting properties are known. [16] It is tempting to speculate on the existence of disorder-order transitions in α_t-$(ET)_2I_3$ upon cooling which might account for the peculiar temperature-dependence of the magnetic susceptibility χ of this compound as shown in Figure 5. Low temperature studies well above and below the superconducting transition are planned on BM 16 in the near future to clarify this point. ■

References

[1] BEDT-TTF and iodine form a plethora of polymorphic phases denoted by small Greek letters, the electrical conductivities of which range from semiconducting to metallic to superconducting (for an excellent review see reference [2]).

[2] J. M. Williams, J. R. Ferraro, R. J. Thorn, K. D. Carlson, U. Geiser, H. H. Wang, A. M. Kini, M. H. Whangbo, Organic Superconductors (Including Fullerenes); Prentice Hall: Englewood Cliffs, New Jersey, 1992.

[3] G. O. Baram, L. I. Buvarov, L. S. Degtyarev, M. E. Kozlov, V. N. Laukhin, E. E. Laukhina, V. G. Onishenko, K. I. Pokhodnya, M. K. Sheinkman, R. P. Shibaeva , E. B. Yagubskii, Pis'ma Zh. Eksp. Teor. Fiz., 1986, 44, 293.

[4] K. Bender, I. Hennig, D. Schweitzer, K. Dietz, H. Endres, H. J. Keller, Mol. Cryst. Liq. Cryst., 1984, 108, 359.

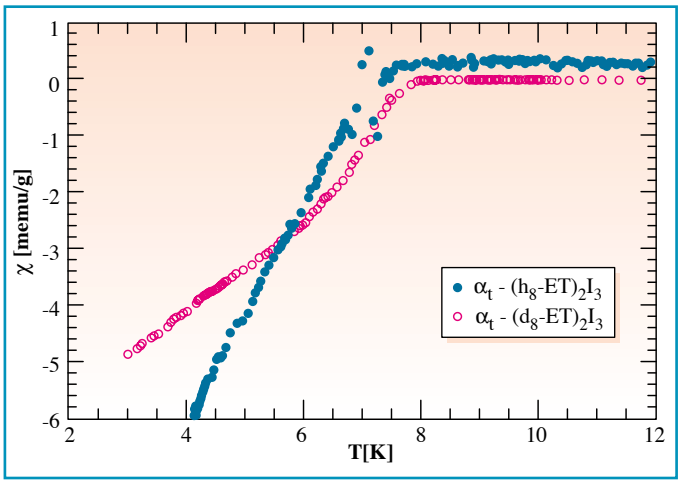

Fig. 5: Superconducting transition curves of protonated and fully deuterated α_t-$(ET)_2I_3$ as determined by AC-susceptibility.

[5] J. Moldenhauer, H. Wachtel, D. Schweitzer, B. Gompf, W. Eisenmenger, P. Bele, H. Brunner, H.J. Keller, Synth. Met., 1995, 70, 791.

[6] Y. Ueba, T. Mishima, H. Kusuhara, Eur. Pat. 0407807 A2, 1990.

[7] K. Kawabata, K. Tanaka, M. Mizutani, Adv. Mat., 1991, 3, 157.

[8] a) E. E. Laukhina, V. A. Merzanow, S.I. Pesotski, A.G. Khomenko, E. B. Yagusbskii, J. Ulanski, M. Kryszweski, J. K. Jeskza, Synth. Met. , 1995, 797. b) J. Ulanski, A. Tracz, J. K. Jeszka, E.E. Laukhina, A. Khomenko, P. Polanowski, D. Staerk, H. Helberg in Electrical and Related Properties of the Organic Solid State, R. W. Munn, A. Miniewicz, and B. Kuchta (Eds.), Kluwer Academic Publishers, Dordrecht, 1997, pp. 241 - 257.

[9] a) H. Müller, Y. Ueba, Bull. Chem. Soc. Jpn., 1993, 66, 32. b) H. Müller, D. G. Xenikos, Synth. Met., 1997, 85, 1461. c) H. Müller, S. O. Svensson, A. N. Fitch, M. Lorenzen, D. G. Xenikos, Adv. Mat., 1997, accepted for publication.

[10] A. C. Larson, R. B. von Dreele, Los Alamos Laboratory Rep., 1987, LA-UR-86-784R.

[11] L. W. Finger, D. E. Cox, A. P. Jephcoat, J. Appl. Cryst., 1994, 27, 892.

[12] J. M. Williams, T. J. Emge, H. H. Wang, M. A. Beno, P. T. Copps, L. N. Hall, K. D. Carlson, G. W. Crabtree, Inorg. Chem., 1984, 23, 2558.

[13] V. F. Kaminskii, T. G. Prokhorova, R. P. Shibaeva, E. B. Yagubskii, Zh. Eksp. Teor. Fiz., Pis'ma Red., 1984, 39, 12.

[14] C. W. Mayer, J. S. Zambounis, B. Hilti, E. Minder, J. Pfeiffer, G. Rihs, Synth. Met., 1991, 41, 2251.

[15] A. J. Schultz, H. H. Wang, J. M. Williams, A. Filhol, J. Am. Chem. Soc., 1986, 108, 7853.

[16] H. H. Wang, J. R. Ferraro, K. D. Carlson, L. K. Montgomery, U. Geiser, J. M. Williams, J. R. Whitworth, J. A. Schlueter, S. Hill, M. H. Whangbo, M. Evain, J. J. Novoa, Inorg. Chem., 1989, 28, 2267.

ACKNOWLEDGEMENT

The authors wish to thank Irina Snigireva from the micromanipulation and microimaging laboratory for providing the SEM image.

Supramolecular Organisation of Collagen Fibrils in Human Tissues

C. Mérigoux[1], D. Durand[1], J. Doucet[1], M. Eugène[2] and O. Diat[3]

1 LURE, Orsay (France),
2 Laboratoire RMN, Hôpital Saint-Louis, Paris (France),
3 ESRF, Experiments Division

The very rich SAXS pattern of human dermis reveals a well defined supramolecular organisation of collagen molecules into fibrils and bundles. The quality of dermis used for skin graft can be checked by this technique.

The structure of skin is not well characterised despite the essential protection role played by this tissue against physical, chemical and microbiological aggression. An improvement in our knowledge of the whole structure is crucial for medical applications (graft, substitution, etc.).

Skin is composed of three different layers; epidermis, dermis and hypodermis (Figure 1). The epidermis serves mainly as a chemical barrier (to water permeation for instance) while the dermis provides most of the toughness of the skin and the hypodermis acts as a thermal and mechanical insulator.

The epidermis is mainly made up of cells (keratinocytes) which during their migration from the dermis to the stratum corneum (upper layer of the epidermis) release lipids which aggregate into bilayers in the intercellular matrix of the stratum corneum. These bilayers have been widely studied by electron microscopy and X-ray diffraction. The lower layer of skin, the hypodermis, contributes to the fatty reserves of the body. As far as the dermis is concerned, fibroblasts are the main cells present in a matrix mostly comprising a protein called collagen and also a small amount of proteoglycans and elastin.

The molecular structure of collagen is a triple helix of about 3000 Å length (Figure 2). The tips which are called telopeptides are partially responsible for the connection between molecules. Consequently, molecules are gathered into fibrils and their arrangement is such that two adjacent molecules are parallel and shifted by 652 Å. In the dermis, these fibrils are also parallel and arranged in bundles which are more or less randomly organised in the tissue.

The classical analytical technique of studying skin-type tissues is transmission electron microscopy which provides structural information from 150 Å to several microns resolution. However, samples undergo several treatments before observation (fixation, staining, dehydration, inclusion) and these are known to modify structural parameters in the whole tissue and at

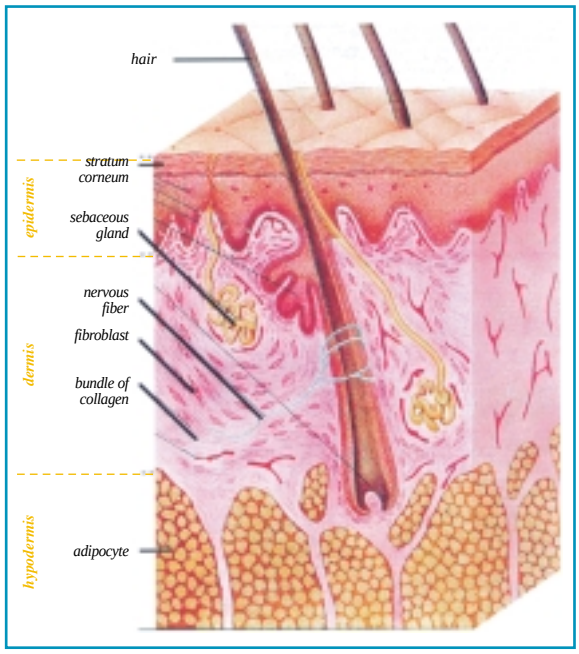

Fig. 1: Schematic representation of human skin (from M. Bago et al, Transplantation, 41, 316 (1986)).

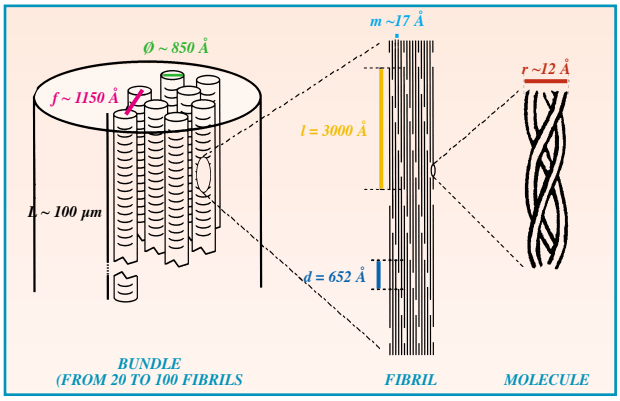

Fig. 2: Supramolecular organisation of collagen into fibrils and bundles of fibrils.

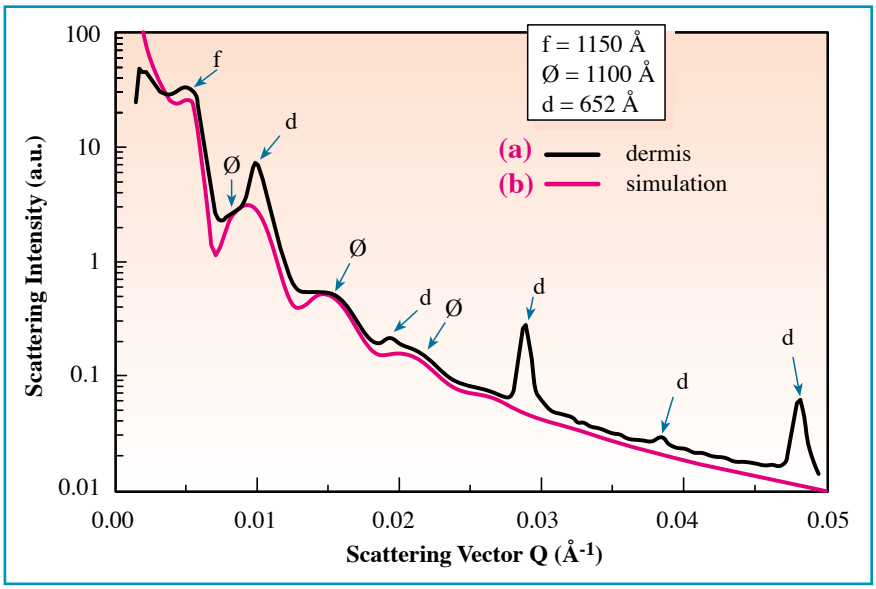

Fig. 3: Scattering pattern for human dermis recorded on ID2 (a) compared to a simulated pattern (b) without taking into account the longitudinal periodicity 652 Å (peaks d). f: peak due to the lateral packing of fibrils. Ø: scattering features due to the cylindrical shape of the fibrils. d: peaks due to the intrafibrillar longitudinal period 652 Å.

each measurement scale [Fullwood]. A complementary technique is therefore needed which does not require chemical modification of the tissue and allows appropriate measurements to be made before the tissue is irreversibly damaged. Such a technique is provided by Small-Angle X-ray Scattering (SAXS), which gives structural information on the packing of the collagen fibrils into bundles on a scale ranging from 10 to 1000 nm. Experiments have been undertaken on fresh untreated human dermis on beam line ID2 at the ESRF. Samples, 1 mm in thickness, were exposed to a high brilliance, highly collimated X-ray beam and diffraction patterns recorded using a multi-wire gas-filled area detector placed at 10 m from the sample, allowing the recording of scattering signals below the mrad angular range. A typical scattering curve **(a)** is shown in Figure 3 after circular averaging and detector corrections. The scattering intensity is plotted versus the scattering vector Q, which is proportional to the scattering angle θ, $Q = 4\pi/\lambda.\sin(\theta/2)$ with $\lambda = 1$ Å. The peaks labelled «d» are well known and correspond to the five first orders of the periodical arrangement of the collagen molecules in fibrils (652 Å period). The envelope of the curve **(a)** is the signature of the scattering from the fibrils themselves; it corresponds to the product of the form factor (oscillations ϕ from which we can extract a diameter of the fibrils, 1100 Å) and the structure factor (correlation peak «f» from which the average distance 1150 Å is determined). The scattering feature «f» had never been observed up to now and the excellent quality of the data has permitted to interpret for the first time the whole scattering pattern in terms of fibril geometry and interfibrillar packing. From a model of these fibrils, packed with a short range position order in a gel matrix, the simulated scattering envelope **(b)** of the scattering curve can be calculated; it is in good agreement with the experimental curve, indicating the correctness of the model.

Similar SAXS experiments carried out on frozen dermis lead to an improved model of the fibrils structure. They consist in a proteoglycan coating surrounding a collagen core of diameter of 850 Å. This type of analysis gives accurate information on the state of the dermis (at the supramolecular scale) and more especially on the quality and nature of the fibrils and how these vary under chemical and physical treatment of the skin tissue (reconstructed tissues, cryoconcentration, etc.). ■

Reference

N.J. Fullwood, K.M. Meek, «A synchrotron X-ray study of the changes occurring in the corneal stroma during processing for electron microscopy», (1993), J. Microscopy, 169, 53-60.

K-EDGE RESONANT INELASTIC X-RAY SCATTERING IN GRAPHITE

P. CARRA AND M. VAN VEENENDAAL*

ESRF, THEORY GROUP (*PRESENT ADDRESS: ARGONNE NAT. LAB., USA)

Recent numerical calculations have provided evidence of the presence of excitonic states in the K-edge emission spectra of graphite, thus identifying a major drawback in the use of resonant inelastic X-ray scattering as a probe of electron band structures.

The scattering of X-rays by a crystal displays unusual anisotropy properties when the response of particular atoms or ions in the lattice is boosted by resonances. Such resonances occur when the X-ray photon energy approaches the value required to excite an inner-shell electron to an empty orbital near the Fermi surface of a solid. Disparate elements - the X-ray polarisation, magnetism of the resonant atoms, and lattice features - then combine to yield a sensitive anisotropy, reflecting lattice properties that otherwise fail to emerge. Electric dipolar transitions usually dominate the scattering process.

High brillance, tunability and polarisation control, available at synchrotron radiation sources, have stimulated a wealth of experimental investigations using X-rays at resonance. In particular, in recent years, a number of experiments have been carried out to test the applicability of resonant inelastic X-ray scattering (RIXS) in determining electronic band structures. Data have been collected from diamond [1,2], B_2O_3 [3], boron nitride [3,4], silicon [5], and graphite [6].

RESONANT SCATTERING AND BAND STRUCTURE

RIXS probes inter-band (valence and conduction) electronic excitations of energy $\omega = \omega_1 - \omega_2$ and momentum $\mathbf{q} = \mathbf{q}_1 - \mathbf{q}_2$, as allowed by the corresponding conservation laws. (The subscripts denote incoming and outgoing photons; $\hbar = 1$). Data are recorded as a function of ω_1 and ω_2, at a given $\mathbf{q}$; usually, the emission spectrum is analysed for a discrete set of ω_1 values, which are taken across an absorption threshold. A typical example, thoroughly discussed in the present report, is provided in Figure 1, where graphite emission profiles are plotted for a few values of the incoming photon energy near the carbon K edge (~ 284 eV). [The spectra are shown for two different experimental geometries: $\alpha = 25°$ and 75°, as described in the caption of Figure 1. This «angular» dependence will not be discussed here. The fluorescence spectrum recorded at ω_1 = 400 eV, that is way above the K edge, is also depicted in Figure 1. We will shortly come back to it.]

A correspondence (band mapping) between the dispersive spectral features of Figure 1 and the graphite band structure, which is depicted in Figure 2 (top panel), is established as follows.

RIXS is accurately described by the lowest Born approximation and proceeds through a core-hole excitation followed by an emission with, in general, an electron relaxation process in between. The total scattering rate (golden rule) reads

$$P_{tot}(\omega_1, \omega_2) = 2\pi \sum_f |U_{i\to f}|^2 \, \delta(E_f - E_i + \omega_2 - \omega_1)$$

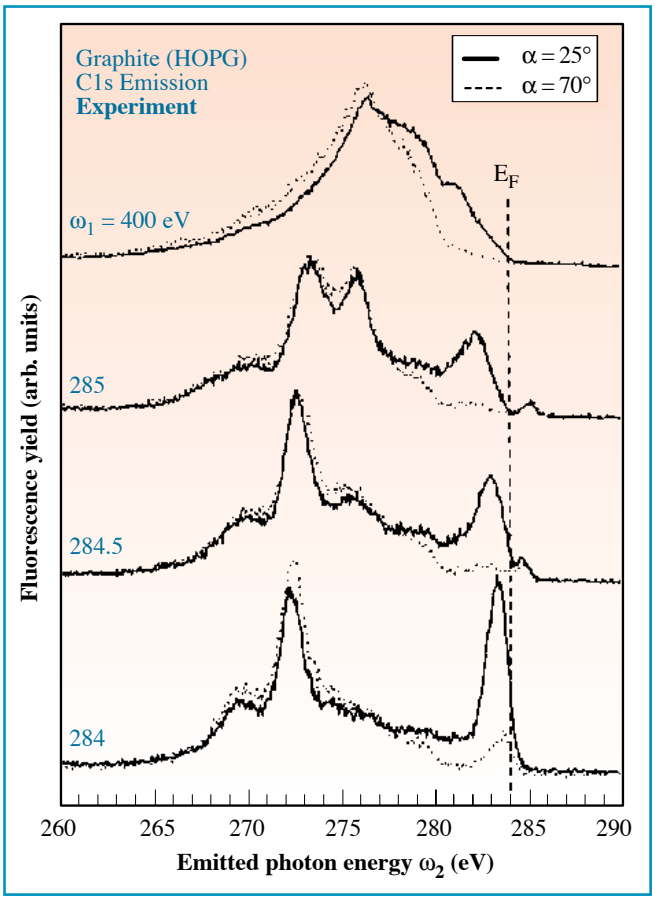

Fig. 1: Graphite RIXS spectra obtained by Carlisle and co-workers, for two different photon take-off angles: α = 25° (solid lines), and α = 70° (dotted lines). Experimental geometry: the scattering plane is perpendicular to the graphite planes; the ingoing photon is linearly polarised in the scattering plane and the outgoing polarisation is not detected. The scattering angle is fixed at 90°. (Reproduced from [6]).

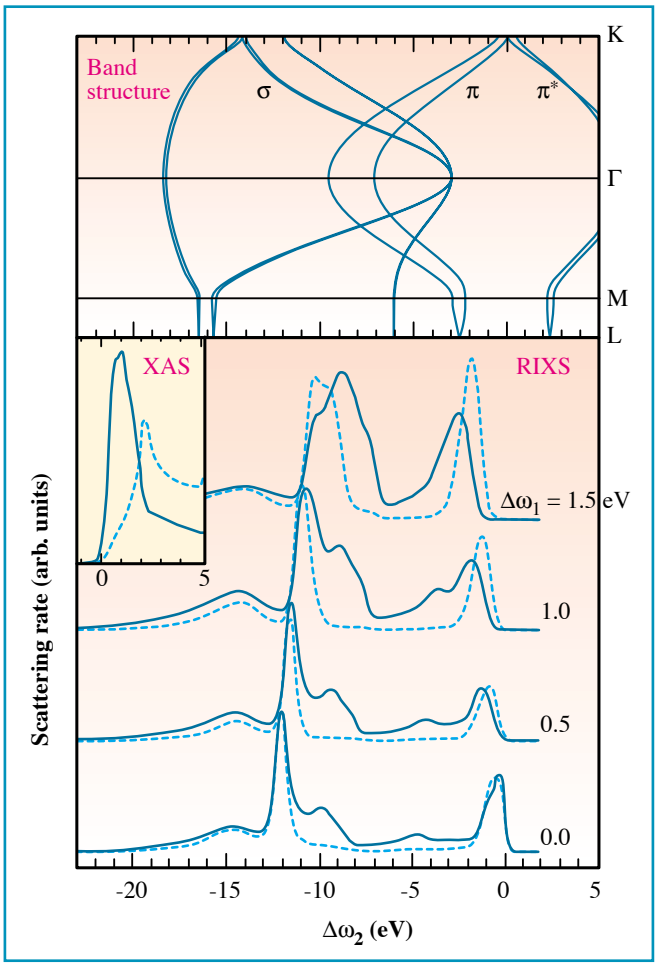

Fig. 2: Upper panel: the band structure of graphite. Lower panel: numerical calculations of the graphite K-edge emission spectra for α = 25°, in the scattering geometry of Figure 1. The independent quasi-particle approximation is given by the dashed lines. The inclusion of a local U= – 3 eV core-hole potential is represented by the solid lines. The corresponding absorption (XAS) profiles are depicted in the inset. (Reproduced from [7]).

where $U_{i\to f}$ denotes the resonant amplitude for a transition from the initial state i to a final state f of the scattering system. (The double-differential cross-section is obtained by multiplying P_{tot} by the density of states of the outgoing photon and dividing by the incoming-photon flux.) Now, assume that the electron states are properly described by a Slater's determinant of Bloch's wavefunctions, i.e. neglect the electron-electron interaction. This approximation, known as 'independent quasiparticle theory', leads to a particularly simple form for the transition amplitude $U_{i\to f}$, the simplifying features being

1. the absence of relaxation effects between absorption and emission,

2. the presence of a single electron-hole pair in the final state.

With reference to the band structure of Figure 2, in graphite the allowed single-pair final states are given by $\pi^*\underline{\pi}$ and $\pi^*\underline{\sigma}$. (Hole states are underlined.)

To compare the data of Figure 1 with the predictions of the independent quasiparticle theory, the present authors have performed numerical calculations of $P_{tot}(\Delta\omega_1, \Delta\omega_2)$ for $\Delta\omega_1$ = 0, 0.5, 1.0 and 1.5 eV, neglecting electron-electron interaction. ($\Delta\omega_1$ and $\Delta\omega_2$ refer to the threshold energy at 284 eV). Only vertical transitions have been considered, thus disregarding the effect of a small but finite photon wave vector. The results are shown in Figure 2 (lower panel, dashed lines). These emission spectra reflect a 1s → π* absorption process, near the K symmetry point, followed by emission from the π and σ bands at about 0, – 11, and – 14 eV. The changes in the spectral profiles, as ω_1 is swept from threshold to 1.5 eV above, are readily explained by following the band structure in the K → Γ direction. Notice that the independent quasiparticle approximation provides no explanation for the emission peak observed at – 8 eV.

To overcome this mismatch, Carlisle and collaborators [6] included a fraction of the fluorescence spectrum (ω_1 = 400 eV) which, as clearly visible in Figure 1, happens to peak at about ω_2 = 276. In our view, their procedure suffers from a twofold inadequacy. Firstly, it introduces a somewhat arbitrary superposition of events which are far removed in energy; and secondly, it relies on a conceptually ill-defined distinction between spatially coherent (near the edge) and incoherent (fluorescence) processes. In fact, it is straightforward to prove that, for Bloch's electrons, P_{tot} (i → f) ~ N with N the number of lattice sites, thus indicating a spatially incoherent process [P_{tot} (i → i) ~ N^2, so that coherence is recovered in the elastic limit.]

ELECTRONIC RELAXATION

To remove the discrepancy described previously, we have included intermediate state relaxation in the form of a screened Coulomb potential acting between the 1s hole and the promoted π* electron. As a result, three steps can be identified in the resonant process

1. 1s → π* absorption exciting the system to its intermediate state;

2. action of the screened Coulomb potential (relaxation) with formation of excitonic states;

3. π → 1s and σ → 1s emission from the relaxed states.

The corresponding numerical emission spectra are shown in Figure 2 (lower panel, solid lines). Notice that an excitonic peak has appeared at about – 8.0 eV, in satisfactory agreement with the observations. This excitonic peak is mainly a result of dipole transitions into the flat-band region between the L and M symmetry points. These states are pulled down by the core-hole Coulomb interaction; consequently, the absorption process is allowed closer to threshold. (We remind the reader that M is a saddle point in the π* band, yielding therefore a large contribution to the graphite density of states.)

The screening of a carbon 1s hole in graphite (a semimetal) has been a point of discussion for nearly twenty years. The lack of agreement between the one-electron density of states and absorption spectra (electron-energy-loss data) was interpreted by Mele and Ritsko [8] as a clear indication of a strong excitonic shift in the final state. Their findings were contradicted by several authors until the

Uppsala group provided inequivocable evidence that, near threshold, the excited electron is localised [9,10]; thus, excitons significantly contribute to electronic screening.

The model we have discussed contains one free parameter: the strength U of the screened Coulomb potential, and our emission spectra have been calculated assuming U = – 3 eV. The same potential strength determines the absorption-peak shift shown in Figure 2 (inset), in agreement with previous calculations and observations. ■

References

[1] *J.-E. Rubensson, D. Mueller, R. Shuker, D.L. Ederer, C.H. Zhang, J. Jia, and T.A. Calcott, Phys. Rev. Lett.* ***64****, 1047 (1990).*

[2] *Y. Ma, N. Wassdahl, P. Skytt, J. Guo, J. Nordgren, P.D. Johnson, J.-E. Rubensson, T. Boske, W. Eberhardt, and S. Kevan, Phys. Rev. Lett.* ***69****, 2598 (1992);*

[3] *W. L. O'Brien, J. Jia, Q-Y. Dong, T.A. Calcott, K.E. Miyano, D.L. Ederer, D.R. Mueller, and C-C. Kao, Phys. Rev. Lett.* ***70****, 238 (1993).*

[4] *J. J. Jia, T.A. Calcott, E.L. Shirley, J.A. Carlisle, L.J. Terminello, A. Asfaw, D.L. Ederer, F.J. Himpsel, and R.C.C. Perera, Phys. Rev. Lett.* ***76****, 4054 (1996).*

[5] *Y. Ma, K.E. Miyano, P.L. Cowan, Y. Aglitzkiy, and B.A. Karlin, [6] J. A. Carlisle, E.L. Shirley, E.A. Hudson, L.J. Terminello, T.A. Calcott, J.J. Jia, D.L. Ederer, R.C.C. Perera, and F.J. Himpsel, Phys. Rev. Lett.* ***74****, 1234 (1995).*

[7] *M. van Veenendaal and P. Carra, Phys. Rev. Lett.* ***78****, 2839 (1997).*

[8] *E. J. Mele and J. J. Ritsko, Phys. Rev. Lett.* ***43****, 68 (1979).*

[9] *P.A. Brühwiler, A.J. Maxwell, C. Puglia, A. Nilsson, S. Andersson, and N. Mårtensson, Phys. Rev. Lett.* ***74****, 614 (1995).*

[10] *R. Ahuja, P.A. Brühwiler, J.M. Wills, B. Johansson, N. Mårtensson, and O. Eriksson, Phys. Rev. B* ***54****, 14396 (1996).*

ACKNOWLEDGEMENT

We are grateful to Y. Petroff for his spirited resistance to the presence of mathematical expressions in the text. Two was the maximum number of equations he recommended ... one turned out to be sufficient.

THE EUROPEAN SYNCHROTRON RADIATION SOCIETY

ESRS
is the Society for you, working on your behalf by

Running SUMMER SCHOOLS
introducing Synchrotron Radiation (SR) techniques to young scientists.

- **Maratea, Italy**:
  1997 - SR in Life Sciences and Chemistry.
- **Luso, Portugal**:
  1998 (6th - 14th May) SR in Materials Science and Physics. We hope to establish a series, e.g.
  1999 Applications of SR in Biological Sciences.
  2000 Applications of SR in Materials Sciences.

Offering a PRIZE
for outstanding SR work by a young scientist.
The Prize is a massive 1500 ECU, to be presented at the Grenoble SR Jubilee conference in November. Details on the WWW at http://fy.chalmers.se/esrs/

Publishing a NEWSLETTER
See the www page if you are a member and have not received yours.

ESRS
needs your membership - otherwise next year will mark both the 10th anniversary of the founding of ESRS and its imminent demise! Use the accompanying form (or the one on the www) to renew or take out membership - PLEASE.

ESRS: MEMBERSHIP FORM

Membership fees

- Scientist 20 ECU - 1 year
- Student 10 ECU - 1 year
- Scientist 40 ECU - 3 years
- Student 20 ECU - 3 years

(1 ECU = 6.58 FF, £ 0.70, 1.96 DM on 18 April 1997)

Eastern European countries:

- Scientist 4 ECU - 3 years
- Student 2 ECU - 3 years
- New Membership
- Renewal

Family name: _____ Title : _____
First name: _____
Address: _____

Tel : _____ Fax : _____ E-mail: _____
Date : _____ Signature :

France: send with your fee in FFr or in ECUS by Eurocheque payable to «ESRS trésorier», to Dr M-Y Adam, ESRS Treasurer, Bat 209d LURE U-Paris Sud, 91405 Orsay Cedex, France.
Germany: Send with a DM cheque to «ESRS», to Dr R. Frahm, HASYLAB-DESY, Notkestieg 85, D-22603 Hamburg, DE. Germany.
Italy: Send with a Lire cheque payable to «ESRS», to Prof. A Mottana. Treasurer: Societa Italiana Luce di Sinchrotrone, via Segre Corrado 2, 00146 Roma, Italy.
United Kingdom: Send with a sterling cheque payable to «ESRS», to Dr Graham Bushnell-Wye, Daresbury Laboratory, Warrington WA4 4AD, UK.

For any queries about ESRS contact the Treasurer, Dr M-Y Adam (Fax: (33) 1 64464148, e-mail: esrsmya@Lure.u-psud.fr), or the secretary Prof. P-O Nilsson, Dept. of Physics, Chalmers Univ.of Tech., S-412 96 Göteborg, Sweden (Fax: (46) 31 165176, email: f1xpon@fy.chalmers.se).

Spin-Resolved Circularly-Polarised Resonant Photoemission

From left to right: N.B. Brookes, B. Sinkovic, L.H. Tjeng.

B. Sinkovic[1], E. Shekel[1*], N.B. Brookes[2], J. B. Goedkoop[2], L. H. Tjeng[3], R. Hesper[3], E. Pellegrin[3], F. M. F. de Groot[3], S. Altieri[3], G. A. Sawatzky[3] and S. L. Hulbert[4]

1 Physics Department, New York University (USA) (*Present address : El-Op. Tel Aviv, Israel)
2 ESRF, Experiments Division
3 Materials Science Centre, University of Groningen (The Netherlands)
4 NSLS, Upton (USA)

The purpose of this paper is to show that it is possible to obtain the spin-resolved valence band of macroscopically non-magnetic transition metal materials (antiferromagnets, paramagnets and materials with disordered magnetic structure). How is this done?

- by using circularly polarised radiation;
- by using electron spin detection;
- by doing the photoemission at a photon energy at resonance with spin-orbit split core levels.

This is illustrated by two examples: nickel metal and copper oxide (CuO). The angle resolved photoemission data on these two materials show that the valence bands are shifted compared to an one electron calculation: in addition structures (around 6eV for Ni and 12eV for CuO) that are not predicted by the one electron calculation appear. These structures called «satellites» are the result of many body effects and are well understood. They are two hole bound states corresponding to $3d^8$ final states. It has been shown in the past that these satellites show very strong enhancement (giant resonance) when the photon energy is tuned to the 2p levels ($h\nu$ = 931.5 eV for Cu and $h\nu$ = 852.7 eV for Ni). This resonance allows the separation of the spectra into final state multiplets (singlets ^1S, ^1D, ^1G - spins antiparallel - and triplet ^3P, ^3F - spins parallel). In this paper, we present results obtained on Ni above the Curie temperature (T_c) and in the case of CuO we show that the top of the valence band is of pure singlet character, supporting the existence of Zhang-Rice singlets in high temperature superconductors.

EXPERIMENTAL ASPECTS

The experiments were performed using the helical undulator [1] Dragon beamline ID12B [2], together with the New York University's spin-resolved electron spectrometer specifically designed for soft-X-ray photoemission experiments [3]. The overall monochromator and electron analyser resolution was set at 1.5 eV. The degree of the circular polarisation at the Ni and Cu L_3 photoabsorption white lines was ~ 0.85 and the detector's spin sensitivity (Sherman function) was 0.07. The angular acceptance of the analyser was ± 4.5 °. The experimental geometry is shown in Figure 1. The spectra were recorded with

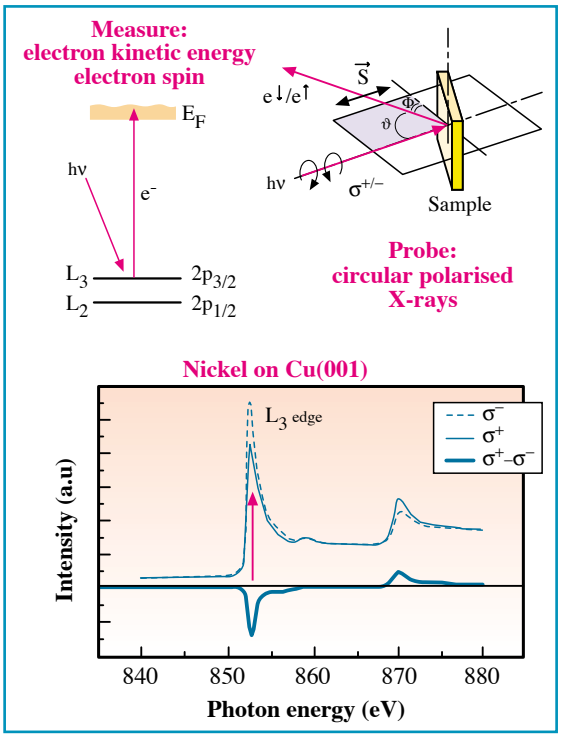

Fig. 1: The upper right panel shows the experimental geometry and the upper left panel the relevant resonant photoemission transition. The lower panel shows the absorption spectra for Ni taken with left and right circularly polarised and the corresponding dichroism spectrum, given by the difference between the spectra taken with left and right circularly polarised.

the four possible combinations of light helicity (σ^+/σ^-) and spin detector channels ($e^{\uparrow}/e^{\downarrow}$, measured simultaneously), in order to exclude any systematic errors.

LOCAL ELECTRONIC AND MAGNETIC STRUCTURE OF Ni BELOW AND ABOVE T_c

Despite a large body of experimental data, a complete description of the finite temperature magnetism remains controversial with some recent results on Ni supporting a Stoner-like behaviour [4], fluctuating band theory [5], or suggesting even more complex behaviour [6]. And as far as the electronic structure is concerned, most of this discussion can be reduced to the question as to whether or not the atomic Hund's rule correlations have survived the strong band formation. Such local exchange interactions, together with the suppression of charge fluctuations due to Coulomb interactions, may account for the failure of mean-field theories to calculate the magnetic ordering temperature (T_c) properly and may give a plausible explanation for the retention of local moments and short range magnetic order above T_c in late transition metals [7].

To provide a better insight in these phenomena, we have investigated the local electronic structure of Ni and its temperature dependence, with special emphasis on the spin-polarisation of the atomic-like 3d orbitals. For this we have used the spin-resolved circularly-polarised 2p (L_3) resonant photoemission technique, a newly developed spectroscopic tool with the unique property that it is capable of measuring the local 3d spin polarisation independent of the orientation of the local moment, which is a necessary condition to study local moments above T_c.

A thick (~100 Å) Ni film was grown epitaxially *in situ* on a Cu(001) surface, yielding $L_{2,3}$ X-ray absorption and spin-unpolarised photoemission spectra identical to those measured previously (Figures 1 and 2) [8]. No Cu signal could be observed in the spectra during all measurements below and above the Curie temperature of Ni (T_c = 627 K) indicating good sample quality. The sample geometry is shown in Figure 1, with $\vartheta = \Phi = 45°$ and normal emission.

The measurements were first performed at room temperature, i.e. below T_c (T = 295 K = 0.47 T_c). In order to obtain an accurate comparison between the spectra taken below and above T_c as discussed later, we purposely demagnetised the room temperature Ni film. The demagnetised state was determined by the reduction of the dichroic effect in the $L_{2,3}$ X-ray absorption spectrum (Figure 1) to a few percent of its fully magnetised value [9].

The thick solid line in Figure 2a shows the valence band photoemission spectra with photon energy tuned at the Ni $2p_{3/2}$ (L_3) white line. This is the sum of the spectra taken with parallel ($\sigma^+\varepsilon^{\uparrow} + \sigma^-\varepsilon^{\downarrow}$) and anti-parallel ($\sigma^+\varepsilon^{\downarrow} + \sigma^-\varepsilon^{\uparrow}$) alignment of the photon spin $\sigma^{\pm}$ and the electron spin $\varepsilon^{\downarrow\uparrow}$. The spectrum reveals primarily the Ni $3d^8$ final states [8], and the peak at 6 eV binding energy is the much discussed satellite of atomic-like ^{1}G character [8,10-15].

More important is to investigate the degree of spin-polarisation, defined as the ratio between the difference vs. the sum of the spectra taken with parallel and antiparallel alignment of the photon and electron spins. The result is presented in Figure 2b, after taking into account the spin detector sensitivity, the degree of circular polarisation and the experimental geometry. We observe that this polarisation is very large, up to about 40%, which is quite remarkable in view of the fact that we are studying a demagnetised Ni film.

It is evident that without the use of circularly polarised light one would not measure a net spin polarisation from a non-magnetised sample since the spin resolved signals from magnetically opposite Ni sites would cancel each other. Yet, it is important to realise that circularly polarised light can only be very effective if a strong spin-orbit splitting is present in one of the atomic subshells under study, because then angular momenta will govern the selection rules [16]. Consequently, direct (non-resonant) photoemission on 3d transition metals would produce little spin signal, because the spin-orbit interaction (of order 0.1 eV) is negligible compared to other interactions like crystal fields and hybridisation (of order 1 eV). To resolve this problem we made use of the $2p_{3/2}$ (L_3) resonance condition (Figure 1) [8]: when the photon energy is near the Ni 2p ($L_{2,3}$) absorption edge, the photoemission consists not only

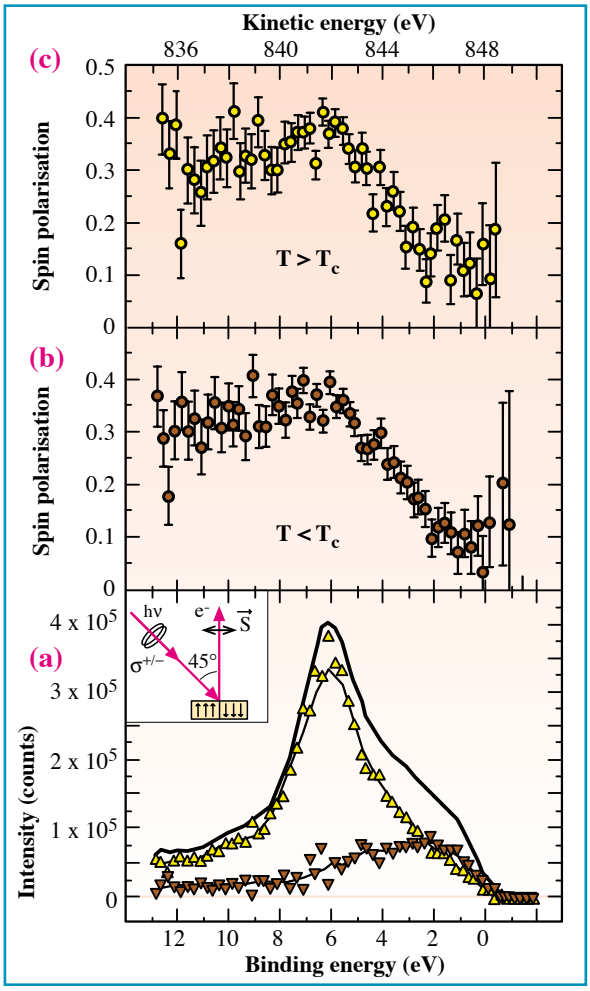

Fig. 2: Spin resolved circular polarised $2p_{3/2}$ (L_3) resonant valence band photoemission spectrum of Ni. Panel (a) shows the spin integrated spectrum (solid line) together with the break down in terms of singlets (Δ) and triplets (▼). Panel (b) depicts the spin polarisation below the Curie temperature (0.49 T_c) and panel (c) above the Curie temperature (1.04 T_c). The inset shows the experimental geometry.

of the direct channel ($3d^9 + h\nu \rightarrow 3d^8 + e$) but also, and in fact overwhelmingly, of the de-excitation channel in which a photoabsorption process is followed by a non-radiative Auger decay ($2p^63d^9 + h\nu \rightarrow 2p^53d^{10} \rightarrow 2p^63d^8 + e$), with the same final state as the direct channel. With the presence of the 2p core level in the intermediate state we now can take advantage of the large 2p spin-orbit splitting (of order 20 eV) and the strong $L_{2,3}$ magnetic circular dichroism (Figure 1) [9]. This forms the main principle of our technique: tuning into one of the two well separated spin-orbit split 2p white lines, circular polarised light produces a spin-polarised 2p core hole, allowing the subsequent Auger decay to produce photoelectrons which are also spin-polarised (with a polarisation depending on the final state). Essential is the fact that the photoelectron carries information concerning the local moment in the ground state, since the probability and degree of spin-polarisation with which the core-hole is created depends on the spin and multiplet character of the valence hole in the ground state, and since the core excited electron is a participator in the Auger decay process. The resulting degree of spin polarisation of the photoelectron is determined by selection rules and details are given elsewhere [17].

Analysis of the data reveals that the peak assigned as the $3d^8$ ^1G state has a degree of polarisation of about + 40%. This compares very well with an analysis of the selection rules [17] for a $3d^9$ initial state configuration, in which the polarisation is found to be + 5/12 (+ 42%) for the ^1S, ^1D, ^1G and - 1/3 * 5/12 (- 14%) for the ^3P, ^3F $3d^8$ final states (neglecting the small 3d spin-orbit interaction). The data therefore show that for 6 eV and higher binding energies only singlet states are present, and that for lower binding energies both singlet and triplet states are present since the polarisation is much reduced but not negative.

Figure 2a shows a break down of the experimental $3d^8$ final states in terms of singlets and triplets, using the above mentioned selection rules and the facts that the measured total intensity is the sum of the two contributions ($I_{tot} = I_s + I_t$) and that the measured total polarisation is a weighted sum of the singlet and triplet polarisation ($P_{tot} = (P_s * I_s + P_t * I_t)/I_{tot}$). The results demonstrate clearly that this type of experiment can unravel the different multiplet or spin states of the valence band of transition metal materials. For Ni we can establish that the singlets are located at much higher binding energies than the triplets and that the triplets extend all the way to the Fermi energy, providing support to the suggestions presented in early spin-unpolarised Auger studies [18,19]. Our data indicate that the on-site Coulomb and exchange matrix elements, and in particular, the Hund's rule still play an important role in determining the energetics of the valence states of Ni despite the strong band formation. Moreover, our data suggest strongly that the ground state has a considerable triplet $3d^8$ character since these extend to the Fermi energy.

The study has also extended the measurements above T_c (T = 653 K = 1.04 T_c). Here we found that the spin integrated spectrum is identical to that at room temperature, shown in Figure 2a. More informative is to look at the spin-polarisation of the high temperature spectra, which is depicted in Figure 2c. It is quite striking that the lineshape of the polarisation function is very similar to that at low temperatures as shown before in Figure 2b. This is also true for the magnitude of the polarisation function, with values up to 40 %. These high temperature results, maybe more so than the room temperature results on the demagnetised sample, clearly demonstrate that this technique is a powerful tool to obtain strong spin-polarised signals from the valence band of transition metal materials which are magnetically disordered and have no net macroscopic magnetisation. Moreover, these results show that the observed polarisation does not depend on the *orientation* of the local moment, but only on the *magnitude* of the local moment, making it an ideal tool for studying local moments in itinerant ferromagnets above T_c.

The lack of change in the local 3d polarisation in going through T_c indicates that also at high temperatures the singlets are located at much higher energies than the triplets and that these triplets extend all the way to the Fermi energy. The latter implies that the ground state has a considerable high spin $3d^8$ character, or in other words, that local moments of 3d character are still present above T_c. This result shows clearly one of the shortcomings of mean-field theory [20] which predict the disappearance of local moments above T_c. More interestingly, our data may provide an insight as to why such theories fail to calculate T_c properly [7]. A consequence of the one-electron approximation is that charge fluctuations are purely statistically distributed since they do not cost extra energy. They are also independent of spin for a non-magnetic system. Our spectra indicate, however, that such a condition is met only for the (low lying) triplets and that charge fluctuations involving singlets are quite energetic, up to 6-9 eV for the ^1G, ^1S like states. It is this neglect of Hund's first rule (triplets lower in energy than singlets) and Coulomb correlations (high energy singlet $3d^8$ satellites) that causes mean-field theories to underestimate the gain in potential energy by keeping the 3d electrons localised relative to the gain in kinetic energy by allowing those electrons to form a band. This underestimation is much more serious in the non-magnetic than in the ferromagnetic case, since in the latter a strong reduction of charge fluctuations can be achieved due to the fact that electrons can move primarily in one of the two spin bands and not in both. Consequently, the energy difference between a non-magnetic and magnetic state is overestimated in mean-field theories, resulting in a too high prediction of T_c.

DIRECT OBSERVATION OF ZHANG-RICE SINGLETS IN CuO

CuO is often seen as a model compound for high-T_c cuprates, since in comparing it with the insulating parent compounds of the superconductors, the magnitude of the insulating gap, the antiferromagnetic superexchange interactions, the basic structural unit (CuO_4), the Cu-O distances, as well as the Cu valence appear to be quite similar. Therefore the characteristics of the first ionisation states in CuO (the two hole final state in photoemission) may be representative for the behaviour of the doped holes in cuprates (ground state) [21].

The angle between the electron emission direction and the light beam was set at 90° (ϑ = 90 °). The CuO sample was prepared *in situ* by high pressure (2-10 mbar O_2) and high temperature (400 °C) oxidation of polycrystalline Cu as described in earlier studies [22-24], yielding unpolarised spectra identical to those measured previously. The measurements were carried out at room temperature.

The top panel of Figure 3 shows the valence band photoemission spectra of CuO with the photon energy tuned at the Cu $2p_{3/2}$ (L_3) white line (hν = 931.5 eV). The thick solid line is again the spin averaged spectrum. Aside from a slightly poorer energy resolution, it is identical to the unpolarised 2p resonant photoemission spectrum in an earlier work [24] and reveals primarily the Cu $3d^8$ final states. The peaks at 16.2 and 12.5 eV binding energy are states derived from the typical atomic-like ^1S and ^1G states, respectively, as explained before [22, 24]. The thin line with open circles is the difference between the spectra taken with parallel and anti-parallel alignment of the photon and electron spins. After taking into account the spin detector sensitivity and the degree of circular polarisation, we observe that this difference is very large, up to 41% of the sum spectrum, which is quite remarkable since we are studying a system with randomly oriented local moments. To verify that this observation is not flawed by instrumental errors, we

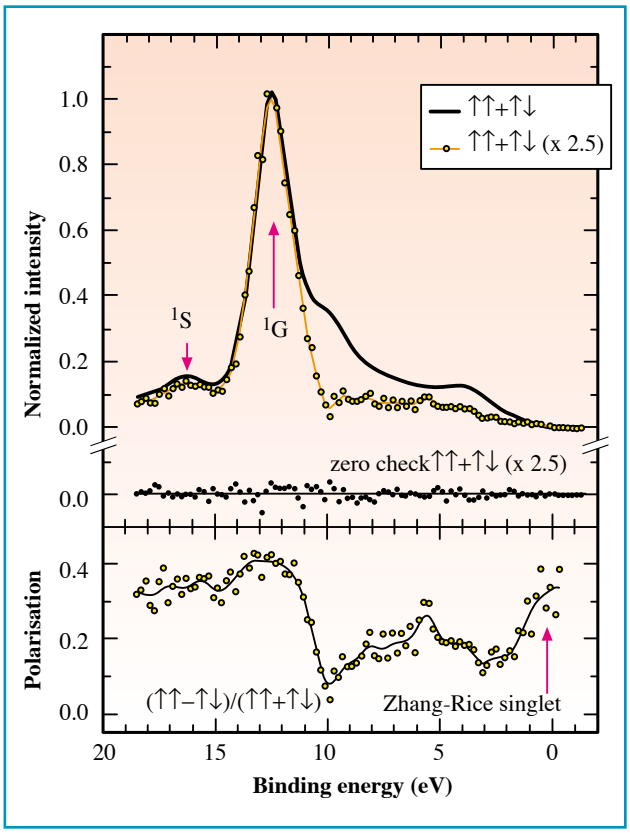

Fig. 3: Spin-resolved circularly polarised $2p_{3/2}$ (L_3) resonant valence band photoemission spectrum of CuO. The thick solid line in the top panel is the spin averaged spectrum. The thin line with open circles is the spin polarisation. The zero check measurement as described in the text verifies a correct experimental set-up.

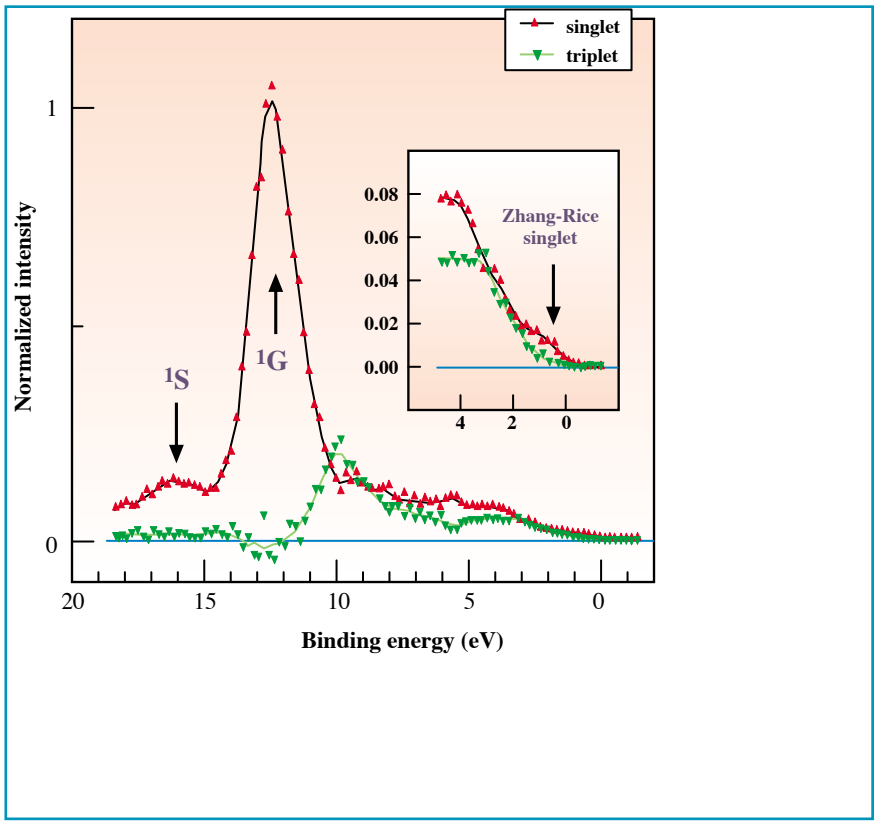

Fig. 4: A breakdown of the spin-resolved circularly polarised $2p_{3/2}$ (L_3) resonant valence band photoemission spectrum of CuO in terms of singlets and triplets. The inset shows that the top of the valence band consists of singlets only.

have performed a zero check experiment. We repeated the measurements under identical conditions with the carbon target replacing *in situ* the gold target of the spin detector. Since the carbon target is not sensitive to the spin of the electron being analysed, any difference signal detected can be ascribed to instrumental asymmetries. As shown in Figure 3, we measured a difference spectrum which is zero, proving that the experiment has been set up correctly and that the above mentioned spin-resolved signals are real.

Figure 3 also shows that the difference spectrum has a different lineshape than the sum spectrum. For further analysis, we represent in the bottom panel of Figure 3 the data in terms of the degree of spin polarisation defined as the ratio between the difference and the sum spectrum. The states assigned as ^{1}S and ^{1}G like have a polarisation of about + 35% and + 41%, respectively. As was the case for Ni this compares very well with the analysis of the selection rules for a $3d^9$ ion. While for 12 eV and higher binding energies only singlet states are present, between 1 and 12 eV the polarisation is much reduced but not negative, indicating the presence of both singlet and triplet states as proposed in earlier studies [22-24]. Quite remarkable is that the polarisation is high again for states located at the top of the valence band, suggesting strongly that they are singlets, i.e. the Zhang-Rice singlets in cuprates. With a value of + 35%, one is tempted to make a comparison with the polarisation of the high energy ^{1}S state (also + 35%) and suggest a common origin. In fact, model calculations [21, 23] showed that both the first ionisation state and the high energy ^{1}S state belong to the $^1A_1$ irreducible representation of the D_{4h} point group, and that the first ionisation state, which is mainly $3d^9\mathbf{L}$ like, acquires some (~7%) $3d^8$ character which is now being probed in this resonant photoemission experiment (**L** denotes an oxygen ligand hole). The calculations [21, 23] also showed that it is the strongly non-cubic environment, present in all cuprates, that makes the first ionisation state to be a singlet. In CuO, the stability of this singlet with respect to other states can be estimated from the width of the high polarisation region, which is about 1 eV.

Figure 4 shows a breakdown of the $3d^8$ final states in terms of singlets and triplets, using the above mentioned selection rules. The results demonstrate clearly that this type of experiments can unravel the different spin states of the valence band of transition metal materials. A quantitative analysis that includes Auger matrix elements could provide a much more accurate modelling of the complicated electronic structure of such strongly correlated systems. In our case, a qualitative analysis is more than sufficient to establish that the first 1 eV of the valence band consists of singlets only, as can be seen from the inset of Figure 4. While much theoretical work has been carried out in the past [21, 25, 26], our study provides the direct experimental support for a meaningful identification of Zhang-Rice singlets in cuprates.

In summary, we demonstrate the feasibility of spin-resolved valence band photoemission on macroscopically non-magnetic transition metal materials, i.e. antiferromagnets, paramagnets and materials with disordered magnetic structure, and show that a very high degree of spin polarisation can be obtained. The combined use of circularly polarised light, electron spin detection and $2p_{3/2}$ (L_3) resonance condition is essential. We have been able to observe a strong spin polarisation in the valence band of Ni [27], not only below but also above T_c. Identification of the separate local singlet and triplet $3d^8$ states provide support for the relevance of Hund's first rule in the formation of the magnetic state in band like late transition metals. Upon crossing T_c, the high spin $3d^8$ states continue to dominate at very low energies, indicating that local moments and short-range magnetic order persist above T_c. We have also been able to unravel the different spin states in the single particle excitation spectrum of CuO [17] and show that the top of the valence band is of pure singlet character, which provides strong support for the existence and stability of Zhang-Rice singlets in high temperature superconductors.

References

[1] P. Elleaume, J. Synchr. Rad. 1, 19 (1994).
[2] J. Goulon et al., Physica B 208, 199 (1995).
[3] B. Sinkovic et al., Phys. Rev. B 52, R15703 (1995).
[4] W. von der Linden et al., Phys. Rev. Lett. 71, 899 (1993).
[5] K.-O. Kamper et al., Phys. Rev. B 42, 10696 (1990).
[6] P. Aebi et al., Phys. Rev. Lett. 76, 1150 (1996).
[7] P. Fulde, Electron Correlations in Molecule, and Solids, Springer Series in Solid-State Sciences 100, (Springer Verlag, 1991), ch. 11.
[8] L.H. Tjeng et al., Phys. Rev. B 48, 13378 (1993).
[9] C.T. Chen et al., Phys. Rev. B 42, 7262 (1990).
[10] C. Guillot et al., Phys. Rev. Lett. 39 1632 (1977).
[11] L.C. Davis and L.A. Feldkamp, Phys. Rev. B 23, 6239 (1981).
[12] R. Clauberg et al., Phys. Rev. Lett. 47, 1314 (1981).
[13] Y. Sakisaka et al., Phys. Rev. Lett. 58, 733 (1987).
[14] T. Kinoshita et al., Phys. Rev. B 47, R6787 (1993).
[15] A. Kakizaki et al., Phys. Rev. Lett. 72, 2781 (1994).
[16] B.T. Thole et al., Phys. Rev. Lett. 55, 2086 (1985).
[17] L.H. Tjeng et al., Phys. Rev. Lett. 78, 1126 (1997).
[18] J.C. Fuggle et al., Phys. Rev. Lett. 49, 1787 (1982).
[19] G.A. Sawatzky, in Auger Electron Spectroscopy, edited by C.L. Briant and R.P. Messmer, Treatise on Mater. Science and Techn., Vol. 30, (Academic, 1988) p. 167.
[20] E.P. Wohlfarth, Rev. Mod. Phys. 25, 211 (1953).
[21] H. Eskes and G.A. Sawatzky, Phys. Rev. Lett. 61, 1415 (1988).
[22] J. Ghijsen et al., Phys. Rev. B 38, 11 322 (1988); ibid. 42, 2268 (1990).
[23] H. Eskes et al., Phys. Rev. B 41, 288 (1990).
[24] L. H. Tjeng et al. Phys. Rev. Lett. 67, 502 (1991).
[25] F. C. Zhang and T. M. Rice, Phys. Rev. B 37, 3759 (1988).
[26] A. K. McMahan et al., Phys. Rev. B 38, 6650 (1988).
[27] B. Sinkovic et al., (to be published).

ACKNOWLEDGEMENTS

It is a pleasure to acknowledge skilful technical assistance of J.C. Kappenburg, L. Huisman and J.F.M. Wieland. We are grateful to the staff of the ESRF for their support, and in particular R. Mason and J. Klora. We thank C.T. Chen, J.-H. Park and V. Chakarian for making valuable testing facilities available at the AT&T Bell Laboratories Dragon beamline. This investigation was supported by the Netherlands Foundation for Chemical Research (SON), the Netherlands Foundation for Fundamental Research of Matter (FOM) with financial support from the Netherlands Organization for the Advancement of Pure Research (NWO), the Committee for the European Development of Science and Technology (CODEST), the New York University Research Challenge Grant No. 5-201-396, and the National Science Foundation Grant No. DMR-9625340. The research of LHT and FMFdG has been made possible by a fellowship of the Royal Netherlands Academy of Arts and Sciences.

EXPERIMENTAL SHAPE OPTIMISATION OF BENT CRYSTALS

U. LIENERT[1,2], S. HARTLAUB[1] AND A. FREUND[1]

1 ESRF, EXPERIMENTS DIVISION, OPTICS GROUP
2 RISØ, MATERIALS RESEARCH DEPARTMENT, ROSKILDE, DENMARK

We describe below a novel method that allows the slope error of bent crystals to be reduced down to the µrad range.

It is the task of X-ray optics to provide focusing and monochromatisation of synchrotron radiation within an appropriate phase space element prescribed by the experimental requirements. Bent crystals cover a wide range of applications and are used on many ESRF beamlines. To fully exploit the optical properties of bent crystals, the slope error should not exceed the beam divergence due to the source size, which can be as small as 0.5 μrad (FWHM)[1]. Often the thickness of the curved crystal is much smaller than the illuminated length on the crystal and the curvature is produced by application of bending moments at the ends of the crystals.

With using existing techniques, simple bending theory is applied to calculate the width or thickness profile of the bent crystal to achieve the desired crystal curvature [2]. This approach imposes severe requirements on the accuracy of the theory and, more importantly, on the realisation of the model assumptions both regarding the crystal and the bending mechanism. We found that simple bending theory, standard crystal and mechanics manufacturing, and crystal mounting techniques do not meet the high precision required for ESRF beamlines. Although finite element analysis can be used to improve the calculations, the effects of strains in the crystal due to both the growth process and to the mounting technique cannot be predicted.

An empirical method has been developed that allows us to reduce the slope error down to the μrad range without requiring costly and time consuming micro-machining of the crystal or sophisticated bending mechanisms. The basic idea is to first measure the local slope of a reasonably well-designed crystal and then to correct the remaining figure error experimentally by shaping the width of the crystal. The width profile can now be calculated by simple bending theory because the required correction is small compared to the absolute crystal deflection.

MEASUREMENT OF LOCAL CURVATURE

Contrary to mirrors, curved crystals are characterised by the lattice plane orientation rather than by the surface profile. Therefore optical metrology is only an indirect tool. An X-ray tube based set-up was developed and is sketched in Figure 1. Traditionally, the bent crystal is translated through the monochromatic X-ray beam and the shift of the Bragg peak is a measure of the local crystal slope. This method was improved to avoid errors due to the wobble of the translation stage: two characteristic X-ray lines impinging at different positions on the crystal are detected in non-dispersive two crystal geometry. Thus only one peak is obtained when a flat crystal is rocked, but the peak splits when the crystal is bent. The local crystal curvature is then calculated from the peak splitting and the distance of the lines on the crystal. Crystal strains produced by clamping are detected by a peak broadening close to the clamps. Laue geometry with almost normal incidence was chosen in this case to minimise systematic errors. Although errors due to wobble of the translation stage can be avoided, a precise rotation table with a linearity of at least 1 μrad is still mandatory.

A Huber 410 rotation table equipped with a 250 mm long lever arm and a Heidenhain linear encoder meets this

Fig. 1: Sketch of the developed set-up to measure crystal curvature. The symbols denote: Ta - Ag X-ray tube target, Mo - flat crystal monochromator, $K\alpha_1$, Kβ - utilised characteristic X-ray lines, Sl - slits, Cr - bent crystal, Tr - translation stage, Ro - rotation table, De - scintillation detector.

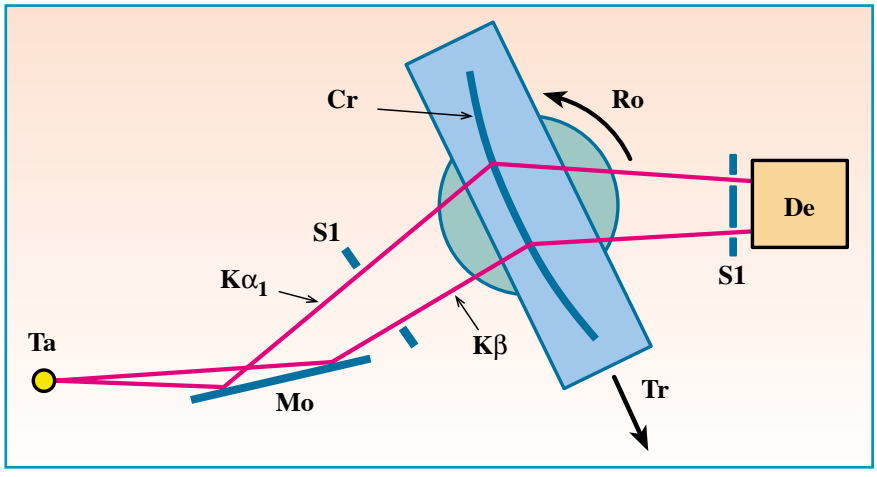

requirement. Figure 2 shows the measured bending radius and slope error of a sample crystal. The X-ray tube based set-up is indispensable for systematic studies but it cannot take into account heat load effects that might occur with synchrotron radiation. However, the variation of the local crystal shape still remains valid if the heat load only changes the average bending radius.

TUNING OF THE LOCAL CURVATURE

Simple bending theory assumes that the local curvature $1/\rho(x)$ is proportional to the local bending moment M(x) and to the inverse of the moment of inertia of the local cross-section I(x). For rectangular cross-sections I is proportional to the beam width and to the cube of the beam thickness. Therefore the crystal width rather than its thickness is profiled to achieve best sensitivity. Crystals of rectangular shape and therefore constant width were bent cylindrically. The width profile for correcting the slope errors is simply given by the ratio of the average to the local bending radii times the average crystal width. Figure 3 shows a width profile thus obtained. To shape the width profile on the crystal, aluminium forms were first produced by a CNC-milling machine. The crystal was then sandwiched between the forms and ground manually following the profile of the forms.

Figure 2 shows the significant improvement of the figure error of the crystal due to the width profiling. This indicates that the grinding did not introduce strains that would affect the local curvature. The line width of the peaks on the X-ray set-up also showed no additional strain.

CONCLUSION

This novel method permits a significant improvement of the slope error of bent crystals, down to the μrad precision. Standard crystal cutting and mounting techniques are sufficient. The method is not limited to cylindrical shapes. Any arbitrary shape (e.g. elliptical, logarithmic spiral) can be produced. ■

References

[1] C. Schulze and U. Lienert, ESRF Newsletter 25, 38 (1996).

[2] see, for example, H. Tolentino, F. Baudelet, E. Dartyge, A. Fontaine, A. Lena, G. Tourillon, Nucl. Instr. and Meth. 289, 307 (1989).

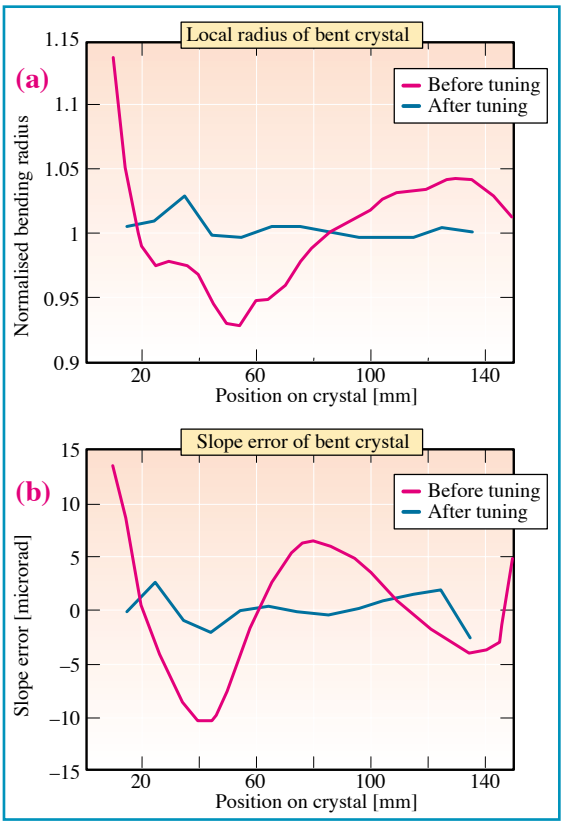

Fig. 2: Comparison of figure error of the cylindrically bent crystal before and after width profiling. (a) normalised local bending radius $\rho(x)/\rho_0$ - the average bending radius was ρ_0 = 50 m. (b) slope error.

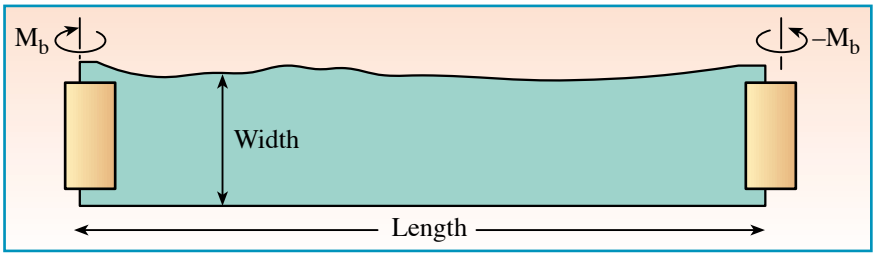

Fig. 3: A width profiled crystal. The crystal is 200 mm long, 1 mm thick and on average 40 mm wide. The crystal clamps and applied bending moments are indicated.

ACKNOWLEDGEMENTS

We acknowledge in particular the skilful crystal grinding by J.P. Vassalli and the continued support at the X-ray set-up by R. Hustache. M. Kretzschmer programmed the CNC machine and the High Energy Group contributed scientific and practical support.

HERCULES 1998

The 8th session of the HERCULES course (Higher European Research Course for Users of Large Experimental Systems) will take place at the Maison des Magistères, CNRS Grenoble,

from 22 February to 3 April 1998

- session A: 'Neutron and synchrotron radiation for physics and chemistry of condensed matter'
- session B: 'Neutron and synchrotron radiation for biomolecular structure and dynamics'

Deadline for application: 17 October 1997

New: in 1998 a limited number of **non-European applications** will be accepted to follow the **session B course**.

Information and application forms will be available at the beginning of July from:

Secrétariat HERCULES:
M-C Simpson
Maison des Magistères
CNRS - BP 166
38042 Grenoble Cedex 9
(e-mail: simpson@polycnrs-gre.fr)